

DEVELOPMENT AND FINITE ELEMENT ANALYSIS OF A
MAGNETORHEOLOGICAL ELASTOMER FOR STIFFNESS VARIATION IN A
SOFT MANIPULATOR

by

Burcu Seyidođlu

B.S., Mechanical Engineering, Bilkent University, 2018

Submitted to the Institute for Graduate Studies in
Science and Engineering in partial fulfillment of
the requirements for the degree of
Master of Science

Graduate Program in Mechanical Engineering

Bođaziçi University

2021

ACKNOWLEDGEMENTS

I would like to express my sincere gratitude and admiration to my advisor Prof. Evren Samur. Thank you for always inspiring and motivating me. You have been a tremendous mentor to me with your unwavering support, insightful advices, and immense knowledge. I would also like to thank Prof. Şebnem Özüpek and Prof. Onur Özcan for accepting to be jury members for my thesis defense and generously giving their time though they have busy schedules.

I will always be thankful to Haptics & Robotics Lab members, Cem, Bora, Günay, Kübra, and Uğur for their help and company. I wish to extend my special thanks to my teammates Taylan and Kübra for their contributions. My sincere thanks must also go to İlke and Şeref for their support and camaraderie. I also thank my dear friends Elif, Melek, Simay, and Dilara for their valuable friendship and always motivating me when I feel anxious. I am forever indebted to my precious friend, Öykü, for making even the most miserable moments bearable. Serhat, thank you for the serenity you brought to my life.

Mom and Utku, I could not have done it without your unconditional love and never-ending support. Dad, I genuinely thank you for everything.

This project was in part supported by Boğaziçi University Research Fund Grant Number 17641.

ABSTRACT

DEVELOPMENT AND FINITE ELEMENT ANALYSIS OF A MAGNETORHEOLOGICAL ELASTOMER FOR STIFFNESS VARIATION IN A SOFT MANIPULATOR

Rigid robots and their inadequate adaptation to challenging environmental conditions requires new intelligent systems. This demand has empowered the evolution of soft robots, that have high dexterity, deformability, and compliance. One crucial requirement for soft robots is the variable stiffness as this provides the potential for tuning the forces exchanged with the environment. Adaptation of smart materials, which can undergo stiffness variations because of the applied physical stimuli, is one of the proposed methods in the literature. Magnetorheological elastomers (MREs) are a type of smart material whose rheological behavior can be changed as a result of the applied magnetic field. MREs generally consist of natural or synthetic rubber perfused with micron sized ferromagnetic particles. In this thesis, an isotropic MRE has been developed to provide stiffness variation for a soft manipulator, which is the STIFF-FLOP. A stand-alone MRE module for stiffness variation has been developed, and tested, an intended application of this MRE module to the STIFF-FLOP soft manipulator is proposed. To capture MRE's material behavior adequately, an analytical method currently used in literature has been advanced by further development. The proposed model has then been implemented in a finite element analysis (FEA) software. This FEA model was compared with the existing method, and experimentally validated. Once the developed FEA was validated, it was used to analyze the stiffness change that might occur due to a possible implementation of the MRE module in the STIFF-FLOP. Results indicate that the proposed FEA is capable of capturing the material behavior of the developed MREs. Results also show that the intended application might benefit from MREs by obtaining highly changing stiffness values.

ÖZET

YUMUŞAK MANİPÜLATÖRLERDE DİRENGENLİK DEĞİŞİMİ İÇİN MANYETOREOLOJİK ELASTOMER GELİŞTİRİLMESİ VE SONLU ELEMAN ANALİZİ

Rijit robotların zorlu çevre koşullarına yetersiz adaptasyonları yeni akıllı sistemler gerektirir. Bu gereklilik, yüksek çevikliğe, deformasyona ve uyumluluğa sahip yumuşak robotların evrimini sağlamıştır. Yumuşak robotlar için çok önemli bir gereklilik ise değişken direngenliktir, çünkü bu çevre ile etkileşen kuvvetleri ayarlama potansiyeli sağlar. Dış fiziksel uyarılar sayesinde direngenlik değişimi gösterebilen akıllı malzemelerin kullanılması literatürde önerilen yöntemlerden biridir. Manyetoreolojik elastomerler (MREler), uygulanan manyetik alanın bir sonucu olarak reolojik davranışı değiştirilebilen bir tür akıllı malzemedir. MREler genellikle mikron büyüklüğünde ferromanyetik parçacıklarla elde edilmiş doğal veya sentetik kauçuktan oluşur. Bu çalışmada, STIFF-FLOP adlı yumuşak bir manipülatöre direngenlik değişimi sağlamak için izotropik bir MRE geliştirilmiştir. Bağımsız bir MRE modülü geliştirilmiş, test edilmiş ve bu MRE'nin STIFF-FLOP'a uygulanması önerilmiştir. MRE'lerin materyal davranışını daha kapsayıcı bir biçimde yakalamak için, halihazırda literatürde kullanılan analitik bir yöntem bazı eklemelerle geliştirilmiştir. Önerilen model daha sonra bir sonlu elemanlar analizi (FEA) yazılımına entegre edilmiştir. Bu FEA modeli mevcut yöntemle karşılaştırılmış ve deneysel olarak doğrulanmıştır. Geliştirilen FEA, doğrulandıktan sonra, STIFF-FLOP'ta MRE modülünün olası bir uygulamasıyla oluşabilecek direngenlik değişimini analiz etmek için kullanılmıştır. Sonuçlar, önerilen FEA modelinin, geliştirilen MRE'lerin materyal davranışını yakalayabildiğini göstermektedir. Sonuçlar ayrıca, MRE'lerden yararlanarak yapılması amaçlanan uygulamanın, yüksek oranda değişen direngenlik değerleri elde edebileceğini göstermektedir.

TABLE OF CONTENTS

ACKNOWLEDGEMENTS	iii
ABSTRACT	iv
ÖZET	v
LIST OF FIGURES	viii
LIST OF TABLES	xii
LIST OF SYMBOLS	xiii
LIST OF ACRONYMS/ABBREVIATIONS	xiv
1. INTRODUCTION	1
1.1. Motivation	2
1.2. Objectives of the Study	3
1.3. Thesis Structure	4
2. LITERATURE REVIEW	5
2.1. Stiffness Variation Methods in Soft Robotics	5
2.2. Magnetorheological Elastomers	11
2.2.1. MRE Materials and Production	12
2.2.2. Finite Element Method (FEM) Studies for MREs	13
3. MATERIALS AND METHODS	15
3.1. Overview of the STIFF-FLOP	15
3.2. Theoretical Analysis	16
3.3. Stand-Alone MRE Module	22
3.3.1. Design & Preparation	22
3.3.2. Cantilever Bending Experiments	24
3.4. Finite Element Analysis of the Stand-Alone MRE Module	25
3.4.1. Model Definition	26
3.4.2. Governing Magnetoelastic Equations	28
3.4.3. LiveLink™ for MATLAB®	29
3.5. Application of the MRE Module to the STIFF-FLOP	31
3.5.1. FEA for the Implementation	32
3.5.2. On-Board Magnetic Field Controller	33

4. RESULTS AND DISCUSSION	37
4.1. Stiffness Change in the Stand-Alone Module	37
4.1.1. Analytical vs. Experimental Results	40
4.1.2. FEA vs. Experimental Results	44
4.2. Stiffness Change in the Proposed Application	48
5. CONCLUSION	51
5.1. Contributions and Originality	51
5.2. Outlook and Future Work	52
REFERENCES	54

LIST OF FIGURES

Figure 2.1.	Main subgroups of common stiffness modulation methods.	6
Figure 2.2.	Curing process of isotropic and anisotropic MREs. Red arrows show the formation of chain-like structures aligned with applied field direction.	13
Figure 3.1.	Front view (left) and side view (right) of a single unit of the STIFF-FLOP soft manipulator.	16
Figure 3.2.	Schematic showing the cantilever beam and the parallel and normal components of \mathbf{M} , \mathbf{H} , and \mathbf{D}	17
Figure 3.3.	A stand-alone isotropic MRE sample with dimensions and production mold.	22
Figure 3.4.	MRE production components and molds.	23
Figure 3.5.	Experimental setup for cantilever bending of MRE samples. Micrometer was used to pull a non-extensible cable which was attached to the tip of the MRE sample.	25
Figure 3.6.	3D model showing magnets (red), an MRE sample (green), surrounding air (grey wireframes), and direction of the magnetic field (red arrows on the xy-plane).	27
Figure 3.7.	Overview of the script used for the resultant force calculations. The blue boxes indicate operations performed in COMSOL [®] while green ones indicate operations performed in MATLAB [®]	31

Figure 3.8.	A single unit of the STIFF-FLOP showing application of the stand-alone MRE module to the central channel.	32
Figure 3.9.	FEA of the MRE module applicable to the STIFF-FLOP. Red arrows showing the direction of the magnetic field, MRE module of 4.5 mm in diameter and 50 mm in length is color coded blue at the center of two square magnets.	33
Figure 3.10.	A single EPM implemented to the STIFF-FLOP for providing external magnetic field when it is on-state. Red arrows show the circulation of magnetic flux.	34
Figure 3.11.	Geometry of a single EPM and its dimensions.	35
Figure 3.12.	The intended application scenario showing the single unit of the STIFF-FLOP merged with developed MRE and external magnetic field controllers (EPMs).	36
Figure 4.1.	Tip force vs. displacement results of the stand-alone MRE modules with volume fractions (f) of 9.09% (top-left), 18.18% (top-right), 27.27% (bottom-left), and 36.36% (bottom-right) under four different magnetic fields (T) (color coded).	38
Figure 4.2.	Comparison of experimental (dotted data points) and analytical (dashed lines) results: Tip force vs. displacement for the MRE sample of 9.09% volume fraction (f) under four different magnetic fields (T) (color coded).	42

Figure 4.3.	Comparison of experimental (dotted data points) and analytical (dashed lines) results: Tip force vs. displacement for the MRE sample of 18.18% volume fraction (f) under four different magnetic fields (T) (color coded).	42
Figure 4.4.	Comparison of experimental (dotted data points) and analytical (dashed lines) results: Tip force vs. displacement for the MRE sample of 27.27% volume fraction (f) under four different magnetic fields (T) (color coded).	43
Figure 4.5.	Comparison of experimental (dotted data points) and analytical (dashed lines) results: Tip force vs. displacement for the MRE sample of 36.36% volume fraction (f) under four different magnetic fields (T) (color coded).	43
Figure 4.6.	Comparison of experimental (dotted data points) and FEA (dashed lines) results: Tip force vs. displacement for the MRE sample of 9.09% volume fraction (f) under four different magnetic fields (T) (color coded).	46
Figure 4.7.	Comparison of experimental (dotted data points) and FEA (dashed lines) results: Tip force vs. displacement for the MRE sample of 18.18% volume fraction (f) under four different magnetic fields (T) (color coded).	46
Figure 4.8.	Comparison of experimental (dotted data points) and FEA (dashed lines) results: Tip force vs. displacement for the MRE sample of 27.27% volume fraction (f) under four different magnetic fields (T) (color coded).	47

Figure 4.9. Comparison of experimental (dotted data points) and FEA (dashed lines) results: Tip force vs. displacement for the MRE sample of 36.36% volume fraction (f) under four different magnetic fields (T) (color coded).	47
---	----

LIST OF TABLES

Table 4.1.	Stiffness [N/cm] values for the stand-alone MRE module.	38
Table 4.2.	Percent change (%) in stiffness [N/cm] values for the stand-alone MRE module obtained from the experiments.	39
Table 4.3.	Stiffness [N/cm] values obtained with the analytical calculations for the stand-alone MRE module.	40
Table 4.4.	Percent error (%) between the analytical and experimental results for the stand-alone MRE module.	41
Table 4.5.	Stiffness [N/cm] values obtained with the FEA model for the stand-alone MRE module.	44
Table 4.6.	Percent error (%) between the FEA model and experimental results for the stand-alone MRE module.	45
Table 4.7.	Stiffness [N/cm] Values for the Intended Application	49
Table 4.8.	Percent change (%) in stiffness [N/cm] values for the MRE applicable to the STIFF-FLOP.	49

LIST OF SYMBOLS

A	Cross sectional area
c	Variable dependant on volume fraction
D	Demagnetization tensor
E	Modulus of elasticity <i>or</i> Young's modulus
E_0	Matrix modulus
f	Volume fraction
F_a	Analytical resultant force
F_e	Experimental resultant force
F_E	Elastic force
F_H	Force due to magnetic interactions
F_T	Resultant force at the tip <i>or</i> FEA resultant force
H	Magnetic field
I	Area moment of inertia
k_e	Elastic stiffness of the beam
k_H	Field-induced stiffness of the beam
L	Free length of the beam
M	Magnetization
M_r	Remnant magnetization
S_{mech}	Mechanical stress
U_E	Elastic energy
U_H	Magnetic energy
U_T	Total resultant energy
y	Tip displacement
θ	Bending angle of the beam
μ_0	Permeability of the free space
$\tilde{\chi}$	The effective magnetic susceptibility

LIST OF ACRONYMS/ABBREVIATIONS

3D	Three Dimensional
BVP	Boundary Value Problem
CIP	Carbonyl Iron Particles
DEA	Dielectric Elastomer Actuator
DOF	Degree of Freedom
EAP	Electro-active Polymer
EPM	Electropermanent Magnet
ERF	Electrorheological Fluid
FEA	Finite Element Analysis
FEM	Finite Element Method
FFA	Flexible Fluidic Actuator
HMA	Hot Melt Adhesive
LMPA	Low Melting Point Alloy
LMPM	Low Melting Point Material
LMPP	Low Melting Point Polymer
LMPW	Low Melting Point Wax
MAP	Magneto-active Polymer
MIS	Minimally Invasive Surgery
MR	Magnetorheological
MRE	Magnetorheological Elastomer
MRF	Magnetorheological Fluid
N/A	Not applicable
PDMS	Polydimethylsiloxane
PLA	Polyactic Acid
SMA	Shape Memory Alloy
SMM	Shape Memory Material
SMP	Shape Memory Polymer
RVE	Representative Volume Element

1. INTRODUCTION

Robots are machines that are skilled and intelligent, and they are used for performing desired tasks for easing human life. Robots' abilities have enhanced a lot over the years; their usage areas, precision of their movements, and the accuracy of motion control have progressed substantially [1]. However, there are still critical challenges remaining especially performing in complex environments: They are lacking the ability of showing large deformations.

Conventional robots and machines consist of rigid structures and stiff materials which restricts their motion capabilities. They can barely show the prosperous multifunctionality that natural organisms spontaneously have [2]. This incompetence paved the way for rigid links or joints of the robots to be replaced by soft materials, which then has brought an emerged research area to the focus: Soft robotics. There are many definitions presented for soft robotics as it is an emerging field of research. An inclusive definition has been made by Chen *et al.* [3] as follows: "Soft robotics is the subject to study how to make use of the softness of an object or a piece of materials or a system for building a robot by satisfying a required softness to both its environment and its receiver." This definition slightly differs from that in the literature as it highlights the concept of softness; the deformation of soft matter and how to control this to accomplish robotic functions. It is possible to engage softness in various ways such as using soft and deformable materials, soft textures, soft actuators, or hybrid systems. All of these can provide enhanced interactions with the environment.

As soft robots have high dexterity and compliance, this comes with some challenges such as effective interaction with surroundings, control of the soft body motion, and simulation. However, the core challenge in soft robotics research is the provisioning of adjustable stiffening as this provides the potential for tuning the forces exchanged with the environment. Compliant state empowers the soft robots to adjust and conform to their surroundings, whereas a stiff state is required to transfer force, to sustain load, and to have precise motion. Thus, tuning of the stiffness has to be performed on

demand and in an ideal case, there should not be any deformation to the soft robot as well.

The variation in stiffness has been achieved through having many stiffening mechanisms and the two main approaches are categorized as the use of active actuators specialized in an opposing manner and the use of semiactive actuators which can adjust their elastic characteristics [4]. Adaptation of smart materials, which can undergo stiffness variations because of the applied physical stimuli, to the soft robots and manipulators is one of the proposed methods in the literature. Magnetorheological (MR) fluids are a type of smart fluid whose rheological behavior can be altered by applying a magnetic field. The use of MR fluids is currently limited by some disadvantages such as particle degradation and controllability issues, which makes another MR material more suitable for tunable stiffness: Magnetorheological Elastomers (MREs).

MREs are generally composed of micron-sized ferromagnetic particles perfused into a natural or synthetic rubber [5]. They are one of the promising options for stiffness variation of soft robots due to their field-dependent behavior producing high stiffness change in milliseconds [6]. In this thesis, an isotropic MRE was developed to provide stiffness variation to a soft manipulator, which is the STIFF-FLOP [7] and a multiphysics FEA was employed to investigate the unique behavior of MREs with a possible application in soft robotics.

1.1. Motivation

The central hypothesis motivating this research is that higher range of stiffness variation and fast response are crucial features for soft manipulators in terms of adjusting the body for changeable external conditions and increasing the mechanical motion capabilities, and that an MRE can be applied to these manipulators to provide these properties.

The STIFF-FLOP soft manipulator [7] was chosen as the possible application scenario as there has been no research on the application of MR elastomers on it yet.

The rationale of the proposed research is that the usage of isotropic MREs in the STIFF-FLOP manipulator can help us reach remarkable changing stiffness values and provide faster response than currently available methods. Thus, making it a novel study to conduct in terms of filling in the literature gap and developing a new design to achieve improved stiffness variation.

The long-term goal of this study is to advance the capabilities of the STIFF-FLOP such that it can be used in minimally invasive surgery (MIS) devices with the help of a possible implementation of an MRE, and also providing a FEA study that can be used for various MRE sample sizes, geometries, and varying magnetic fields to be able to observe stiffness variation capabilities at the design stage.

1.2. Objectives of the Study

Objective 1: Developing a stand-alone stiffening MRE module. A stand alone soft module which is made of an isotropic MRE was developed. In addition, an external system to give this design different magnetic fields and control the stiffness was also developed. Successfully, accomplishing this aim informed us about the effect of the MRE implementation on stiffness tuning, and its response time.

Objective 2: Developing a FEA study to analyze stiffness variation from a possible MRE application. The developed FEA study can be used for various sample sizes, geometries, and varying magnetic fields. It made observing the change in stiffness possible prior to an actual implementation, and thus made it easier to analyze the stiffening variation caused by MREs at the design stage.

This study has the potential to lead to the development of a novel isotropic MRE applied to the STIFF-FLOP, which is controlled by an external magnetic field supplier for higher stiffness range, controllability, and fast response. The performed work is innovative because it capitalizes on tunable stiffness of the STIFF-FLOP soft manipulator as a result of implemented MREs, which is not tested and applied before, and can be a pioneer for future developments as FEA will make it possible to analyze

a possible application scenario prior to design stage. The proposed FEA method can be implemented on various MREs and soft manipulators.

1.3. Thesis Structure

The thesis is structured as the following: Chapter 1 provides the background of this study, states the motivation behind it, and clearly outlines the aims. It also includes a brief overview of the thesis format. Chapter 2 includes the literature related to this study. In Chapter 3, overview of the soft manipulator is presented, theoretical background is given, MRE development is stated in detail, and the FEA study is explained briefly. Chapter 4 indicates the resulting stiffness change for the stand-alone MRE module and in a possible application scenario, and discusses these results. Lastly, Chapter 5 highlights the contributions of this study and states the future work.

2. LITERATURE REVIEW

2.1. Stiffness Variation Methods in Soft Robotics

The need for soft robots to be highly deformable and compliant has deepened the research in the use of unconventional materials and structures. The core challenge is the variability and controllability of such deformable and compliant materials and morphologies [4]. For an efficient interaction with the surroundings, it is important to tune stiffness accordingly. There are several ways to adjust stiffness which are generally linked to actuation methods and mechanisms, and they are mainly focused research areas. However, it is also possible to have the desired stiffness change as a result of material deformation, that is the case when working with soft materials-based actuators. Yang *et al.* [8] summarized existing principles under four groups based on their operating principles. These stiffness modulation methods are: jamming-based methods, glass/phase transition-based methods, structure-based methods, and viscosity-based methods. Additionally, a potential fifth method for stiffness variation in soft robots is proposed as acoustic-based methods, which is a promising research area and can provide directions for future developments. However, the main focus of current applications is on wireless actuation; thus, this possible method will not be reviewed here. The detailed diagram of the stiffness modulation methods can be seen in Figure 2.1.

Jamming based systems are one of the most used stiffening mechanisms in soft robotics. There are three major types of jamming that have been widely used. These are granular jamming, fiber jamming, and layer jamming. Granular jamming is the first type of jamming that was explored to use in soft robotics applications, and it is still the most valid one [9]. It is based on the transition from a soft material into a rigid under applied external loading. Generally coffee granules, sand, or gravel are used as the low-density packing material. However, it is not only restricted to granular matter: bundles of threads or planar sheet packing can also be used [9].

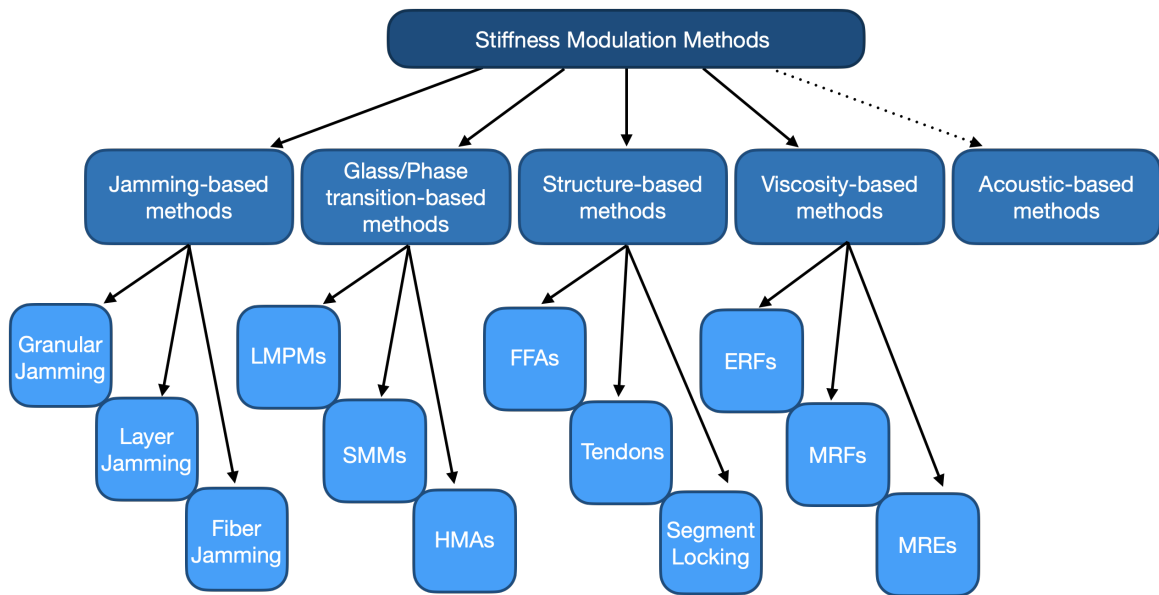


Figure 2.1. Main subgroups of common stiffness modulation methods.

Granular jamming can provide considerable amount of stiffness variation, which makes it easily adaptable to various applications including gripping, end effector of a body, or locomotion. Steltz *et al.* [10] used granular jamming to introduce a new jamming skin enabled locomotion for a soft mobile robot. They used a granular jamming mechanism to modulate the direction, by morphing its shape and achieving locomotion. Based on this foundation, Steltz *et al.* [11] then developed jamming modulated unimorph which again uses jamming as an enabling mechanism. The basic idea behind this linear actuator design is that jamming modulated unimorph uses a discrete number of jamming cells to turn the linear actuator into multi degrees of freedom (DOF) bending actuator. Another jamming based application was a universal gripper which is able to grasp varying types of objects that differs in shape and rigidity [12]. In the developed gripper design, a single mass of granular material was used to substitute individual fingers. The transition between unjammed and jammed states were realized with the help of vacuum, and the gripper was allowed to hold the objects. A later work developed this design by incorporating positive pressure into the system [13]. Positive pressure increased the gripping capabilities in real world applications and decreased the force needed to hold objects. Since they are simple, feasible, and reliable, the use of jamming based technologies in many innovative scenarios has become very common. For the MIS devices, tuning of the stiffness is crucial, as instruments should be flexible

enough to operate effectively. A comprehensive review shows that MIS devices such as endoscopes use jamming based mechanisms widely [14]. The STIFF-FLOP soft manipulator was also incorporated with a granular jamming mechanism to be able to present higher stiffness variation range [15, 16].

The need for considerable amounts of volume of granular material to accomplish significant stiffness changes has increased the search for better alternatives. Layer jamming is one of the proposed methods as it requires less volume than granular jamming and is also lighter in weight. Overlapping layers and structures and the friction force between them enable stiffness change. Santiago *et al.* [17] used mechanical layer jamming for a variable compliance continuum robot section with a new approach inspired by biology, Kim *et al.* [18] presented a novel layer jamming mechanism which can be controlled by confining pressure and highly applicable to MIS devices. A stiffness and shape changing device using a novel multiple chamber inflatable structure was developed by Ibrahimi *et al.* [19], and they also proposed the possibility to wear this system as an orthotic brace. They also measured that this technology could increase overall patient comfort. Some novel applications of layer jamming include hybrid systems like electrostatic layer jamming presented in [20]. They used electrostatic attraction to compress the layers and thus create friction for activating the jamming.

The scalability of layer jamming is questionable in some cases especially in small or slender devices as at stiffer states this requires bigger workspace. Therefore, fiber jamming can be a solution for these workspace and scalability problems. Jadhav *et al.* [21] presented a fiber jamming module consisting of axially picked fibers which can provide the flexural stiffness. They used this as a part of a kinesthetic force feedback haptic glove. Brancadoro *et al.* [22] studied fiber jamming applied to cylindrical components to develop variable stiffness structures. They used fibers of different materials and tested them under bending conditions. They discovered that geometrical features of fibers are least important when compared to surface roughness; and thus they have developed some preliminary guidelines for fiber jamming mechanisms.

Another stiffness modulation strategy for soft robots can be classified as material glass transition or phase transition-based stiffness variation. Low melting point materials (LMPMs) like low melting point alloys (LMPAs), low melting point polymers (LMPPs), and low melting point waxes (LMPWs); shape memory materials (SMMs) like shape memory alloys (SMAs) and shape memory polymers (SMPs); and thermoplastics are some examples of the glass/phase transition-based materials. Mechanical properties of such materials undergo changes as a result of thermal inputs. Glass transition and melting transition temperatures of these materials can cause significant changes in elastic moduli [8]. Cheng *et al.* [23] explored a novel soft material which is thermally tunable, self-healing wax-coated composite. This design was proposed to be used in robotic locking joints which can achieve a high range of stiffness. It was also observed that the developed material has self-healing properties as an effect of being wax-coated and heating. In this study, a foam beam was produced and filled with wax. Copper wire wrapped around it in order to provide the heat. When wax melted from the applied heat, the foam bent accordingly. In another study, it was reported that a glass transition-based polymer can be used for a dramatic decrease in the elastic modulus with the help of an external thermal input [24]. They observed that cooling and heating can affect the mechanically dynamic behavior of nanocomposites. Gandhi and Kang [25] used LMPP layers to vary the flexural bending stiffness by increasing its temperature through the glass transition. It is observed that a multi-layered beam's flexural stiffness is greater when at lower temperatures. A novel stiffness variable actuator which consists of a dielectric elastomer actuator (DEA) and LMPA inserted silicone was also developed [26]. It uses Joule heating to switch between soft and rigid states.

Another application of glass transition-based stiffness change was performed by Yang *et al.* [27]. A bioinspired robotic finger design was developed with an SMP joint and the thermal energy of this SMP was controlled. When the temperature is around the glass transition temperature, the elastic modulus can be modulated. Yuen *et al.* [28] created variable stiffness fibers using thermally responsive polymers. Experiments were performed on different thermoplastics with varying glass transition temperatures and integration of them into fabrics were also realized. Chenal *et al.* [29] developed fibers

that are able to change their stiffness as they are made of SMA covered with a thin layer of SMP. They studied whether wearable applications could use this to have stiffness modulation. There are also other studies which focus on the use of these materials for reconfigurability or self-healing. A compact origami-based robot design is proposed in [30], which can change the stiffness of its joints. To be able to control the stiffness of the design they used an SMP with a stretchable heater. Hot melt adhesives (HMAs) are also categorized under phase transition-based stiffness modulation materials. They are thermoplastics with temperature dependent adhesiveness, this property is used in [31] to link passive external objects with the robot's body and the self-reconfigurability of the structure is observed. All these materials and plastics have demonstrated their potentials for the stiffness modulation in soft robots; however, they have some drawbacks as extensive periods of time is required for these processes as well as the need for a thermal input for unstiffening, which increases the overall complexity of the system. These are some limitations especially in the case of MIS devices and other applications that require a fast response.

Third class of stiffness modulation methods is the structure-based method. While other methods generally rely on the intrinsic rigidity tuning of the materials, this method differs from the others as it can also be achieved through structural designs [8]. Flexible fluidic actuators (FFAs), and tendon-driven actuators arranged in an antagonistic manner are some main technologies that can be categorized under structure-based stiffness mechanisms. FFAs are inflatable structures which are actuated by fluid, and can be deformed into desired shapes by adding additional materials and designing structures accordingly [4]. FFA based technologies enable stiffening variation with the help of designing structural asymmetric deformations arranged according to desired directions. The well-known McKibben actuators are considered as a special type of FFAs. As explained in [32], contracting and extending rubber actuators were developed based on a McKibben actuator. Since FFAs have low stiffness, they were combined with different rubber actuators to provide a bending mechanism. These bundled actuators have higher stiffness compared to the ordinary fluidic rubber actuators. Another variable stiffness robotic hand was developed in [33] using pneumatic soft rubber actuators, this tendon-driven robot hand can adjust its stiffness according to the input air pressure.

A combination of different types of actuation techniques can also help us modulate stiffness. The antagonistic arrangement method provides variable stiffness achieved through the use of active parts that are applied in opposition to one another or are paired with passive structures [4]. Shiva *et al.* [34] developed a continuum silicon-based manipulator inspired by muscular structures of the octopus. The developed design has an antagonistic actuation arrangement, tendons in the structure works coordinately with the manipulator's pneumatic actuation system and with these two actuation mechanisms it is possible to change the stiffness of the soft manipulator. A similar work is presented in [35], again inspired by the actuation principle of octopus arms. A soft, inflatable manipulator was developed and antagonistic arrangement of tendons and pneumatics actuated the manipulator. This arrangement helps with both movement and stiffness variation of the manipulator. Another design of a continuum manipulator developed with the antagonistic actuation of tendons and radial FFAs [36]. The inspiration for this design came from muscle layers found in muscular hydrostats. They reported that the developed soft manipulator was able to extend, contract, and bend in three-dimensional (3D) space and stiffness could be changed by the manipulation of radial FFAs and longitudinal tendons. The limitations of these designs are the requirement for an air pressure input and the miniaturization problem.

When the scale becomes delimitative for fluidic actuators in an antagonistic arrangement, there are other techniques to achieve stiffness variation with simpler structures like SMAs. The arrangement of braided sleeves and SMAs used in [37] is another way to achieve stiffness variation. Another study [38], similar to previous one, used SMA springs and longitudinal cables to actuate the octopus robot whose arms can change its stiffness as a result of simultaneous activation of the whole structure. Usage of EAP rather than SMA [39] with a similar design approach mentioned in the previous study is also another method to achieve stiffness modulation.

Segment locking is also a well-known approach for structure-based stiffness modulation which is specifically used a lot in MIS devices [8]. The basic idea behind this design is pressurizing the cables to lock a segment on a manipulator, and thus provide a change in stiffness. A flexible endoscope based on these phenomenon was developed

in [40], with an outer tube and stiff spines inside that helps to lock. Another study based on segment locking was performed in [41] for a single port robotic surgery device. A unique arrangement of the tendons and links helped to adjust stiffness.

The fourth stiffness modulation technique that will be explained is the viscosity-based methods. Electrorheological fluids (ERFs), magnetorheological fluids (MRFs), electroactive gels are some types of materials that indicate viscosity change based on external electric or magnetic field, and can be used for stiffness modulation. ERFs and MRFs are also called smart materials as they have the feature of undergoing stiffness variations because of the applied physical stimuli [42, 43]. This feature of tunability of viscosity and thus stiffness has influenced researchers to adapt them to soft robotics applications. ERF is used for a valve in [44] to simplify the flexibility of the developed soft robot. However, the usage of ERF is less common, because of the sedimentation issue of the ferroelectric particles [45], and also the need for higher voltages. Their elastomeric version is also much less widespread since it does not provide a useful stiffness change compared to the other methods explained here.

The use of MRFs is also currently limited by some disadvantages such as particle deposition and controllability issues [46], but its use in soft robotics for stiffness modulation is more common when compared to ERF. A soft ribbon with MRF filled microchannels in [47] shows a tunable stiffness even at the low magnetic fields. It was reported that it has the potential to be an alternative way to stiffness control. Another MR material which is also highly suitable for tunable stiffness is the MREs. When subjected to a magnetic field, MREs exhibit a unique field-dependent material feature, and they also overcome major problems that MRFs have like particle degradation and issues with sealing [46]. They will be explained in detail in Section 2.2.

2.2. Magnetorheological Elastomers

MREs are composite materials that contain magnetic particles randomly distributed or aligned in a certain direction within an elastomer matrix [48]. The unique feature of having controllable stiffness and damping in response to an external magnetic

field paves the way for development of various MRE devices such as vibration isolators, dampers, and sensors [49, 50]. The MR effect defines the change in Young's or shear modulus under applied field with respect to the value without a magnetic field. MREs stiffening and compliance speeds are higher than the other proposed methods, which means they can provide fast response and are more controllable, making them more suitable for tunable stiffness [46, 51]. All of these features indicate that MRE has an enormous potential as a stiffness variation material, and its implementation into the soft manipulators can be a promising and novel solution.

2.2.1. MRE Materials and Production

MREs are comprised of three main components; an elastomer matrix, additives, and magnetic particles [52, 53]. The magnetic particles should have low remnant magnetization, high saturation magnetization, and high permeability [54]. MR effect is maximized when the particles with high permeability are used in the compound. This is due to the fact that the particles easily attract small magnetic leakage fields in the elastomer matrix [52]. Rheological behavior of MREs is determined by many parameters such as particle size, volume fraction of the particles, applied magnetic field and used polymer matrix [55–57].

The main classification of MREs is based on their curing process. An external magnetic field applied during the curing process aligns the micro/nano-sized particles in the direction of the magnetic field, forming chain-like structures inside the soft polymer matrix, resulting in an anisotropic MRE; if no external magnetic field is applied during the preparation, particles are randomly distributed, resulting in an isotropic MRE [42]. The difference between curing process of isotropic and anisotropic MREs and their microscopic structures can be seen in Figure 2.2. There are many studies showing that anisotropic MREs have a stronger magnetorheological effect than isotropic ones [58, 59]. When volume fraction was investigated, if the content of the magnetic particles is too low, then it becomes harder to cause a remarkable MR effect. Some studies reported that the optimal volume fraction of particles is around 35-40% [52, 60]; while some others found that a stronger MR effect was seen when it was around 27% [61–63].

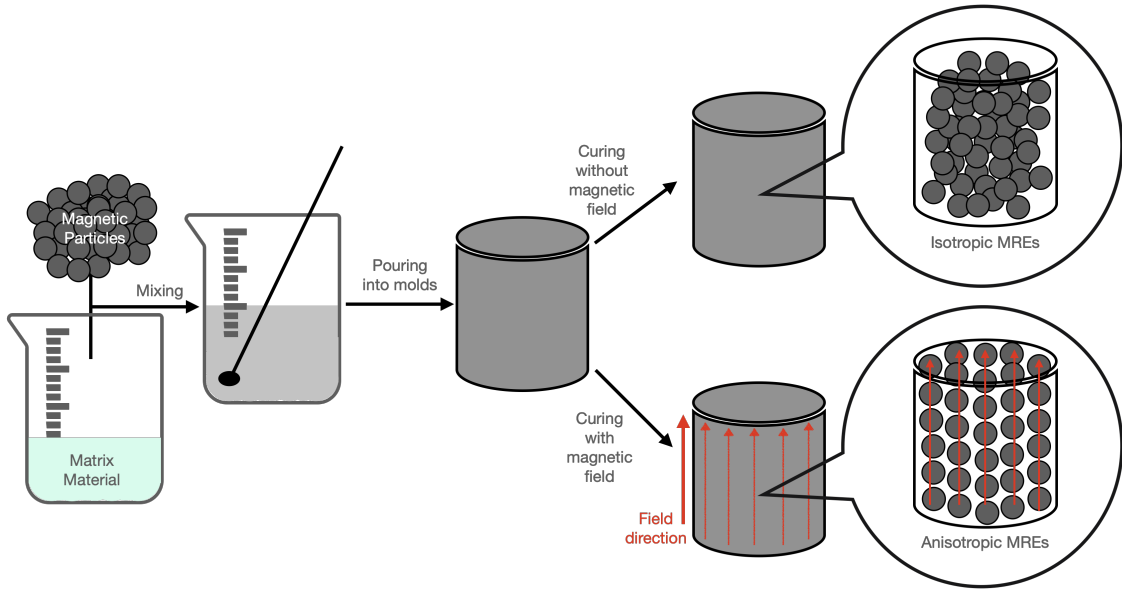


Figure 2.2. Curing process of isotropic and anisotropic MREs. Red arrows show the formation of chain-like structures aligned with applied field direction.

2.2.2. Finite Element Method (FEM) Studies for MREs

There are few studies focusing on finite element method (FEM) model of MREs. Roche *et al.* [64] compared the actuation capabilities of hard- and soft-MREs. Schubert and Harrison [65] compared the mechanical response of MREs with different volume concentrations under different deformation modes to observe large-strain behavior. Halder *et al.* [66] embedded constitutive relations for magneto-active polymers (MAP) into FEA by modeling a 2D plate with a hole geometry and observed the different loading scenarios. Sun *et al.* [67] used the representative volume element (RVE) method to explore the mechanical properties of anisotropic MREs, and they discovered that the shear modulus increases with the increasing magnetic field. A 3D FEA was performed by Syam *et al.* [50] for a particle level (micro-scale) which analyzes the influence of magnetic field of both axial and torsional stiffness. Kalina *et al.* [68] also performed a micro-scale analysis for anisotropic MREs at finite stresses using a continuum formulation for the magnetomechanical boundary value problem (BVP). They observed deformation dependent behavior of MREs with chain-like structures depend strongly

on the particle arrangement and the applied magnetic field. Another FEA study [69] performed an MRE base isolator to examine the magnetic field distribution inside an MRE device. The majority of these studies were done in micro-scale, and some were done for MRE-based isolators or vibration absorbers. None of these studies have focused on developing a 3D milli-scale finite element model for analyzing MREs stiffness variation capability for a soft robot application.

3. MATERIALS AND METHODS

The primary focus of the study is to build an MRE for stiffness variation in a soft manipulator, and develop a FEA model for discovering its effectiveness before an actual implementation. To accomplish these aims, cantilever bending behavior of MREs was investigated in terms of its dependency on the volume fraction, f , of magnetic particles and the applied external field. Additionally, a FEA model was developed for the produced samples to investigate their field-dependent response to varying magnetic field. This FEA was also used to investigate the possible MRE application to a soft manipulator.

The soft manipulator that will be used for the application scenario was chosen to be the STIFF-FLOP, which is explained in Section 3.1. Theoretical analysis is given in Section 3.2, production method of the MRE is described in Section 3.3, developed FEA is briefly explained in Section 3.4, and lastly, an overall design suggestion is given in Section 3.5.

3.1. Overview of the STIFF-FLOP

The STIFF-FLOP is a unit of a modular manipulator developed by Cianchetti *et al.* [7] for MIS operations. The developed manipulator has three pneumatic chambers and one central channel reserved for the additional applications such as carrying the camera cables if mounted or an extra implementation for a stiffness modulation mechanism or system. Three chambers are actuated using FFAs, which enables the manipulator to have omnidirectional bending and elongation. The silicone tubes are covered with braided structures which help with further bending. The structure and dimensions of the STIFF-FLOP can be seen in Figure 3.1.

To date, stiffness variation of the STIFF-FLOP is achieved through jamming-based mechanisms, or hybrid antagonistic actuation method which includes both granular jamming and tendons for stiffness variation. Granular jamming allowed to increase

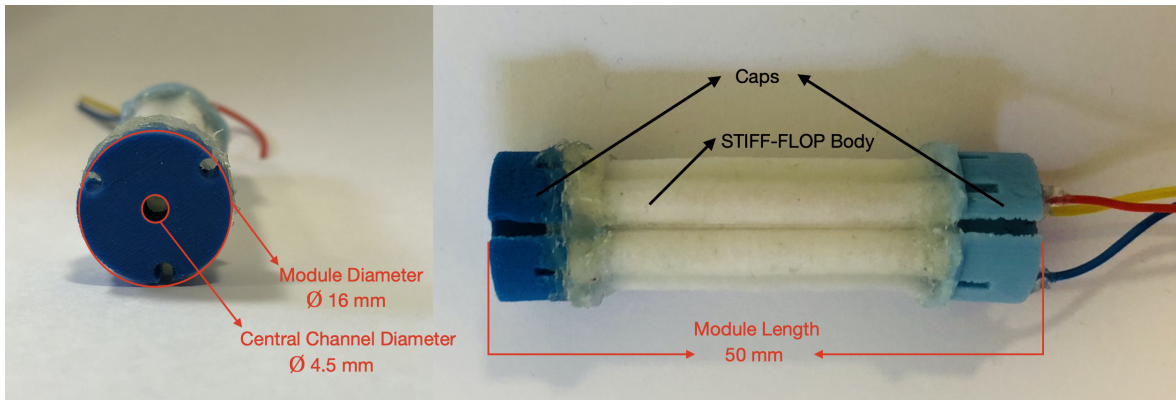


Figure 3.1. Front view (left) and side view (right) of a single unit of the STIFF-FLOP soft manipulator.

the stiffness up to 37% in [70], and 12.4% in [71] for the 90 degree bending position. The central channel of the STIFF-FLOP units where the granular jamming mechanism was implemented is 8 mm in these studies [70,71]. The hybrid system consists of braided tendons, and granular jamming implemented into the central channel of 9 mm, provided a 17.4% increase in bending scenario when there is no tension in tendons [34]. If there is also tension in tendons, then it is possible to increase the stiffness change up to 30.7% [34]. These methods were able to provide sufficient stiffness variation ranges; however, the need for pneumatic input and the slower unstiffening time were the drawbacks especially for MIS operations. An MRE implementation in the central channel of the STIFF-FLOP with an on-board magnetic field controller can eliminate these disadvantages. This promising stiffening technology has not been tried on the STIFF-FLOP yet. It could be a novel design which would allow more efficient MIS operations by decreasing the overall system complexity, and also remove the need for continuous power supply.

3.2. Theoretical Analysis

The elastic modulus, E , of MREs indicates a remarkable change with respect to the applied field, and it is also dependant to the volume fraction, f , of the magnetizable particles that it contains. To accurately analyze the influence of the applied field and f , it is important to present an analytical model which defines the increment in E .

There are two main approaches that try to explain MREs magnetoelasticity: theories that use continuum mechanics point of view, and statistical or kinetic theories which use energy-based method to derive magnetoelastic properties. We have developed our governing magnetoelastic equations based on a study performed by Lockette *et al.* [72] which focuses on the cantilever bending behavior of MREs. In order to predict MRE's response under changing magnetic field, they used the beam theory model with elastic strain density, and coupled it with demagnetizing effects in the magnetic energy density. A schematic showing the cantilever beam that is investigated can be seen in Figure 3.2, where \mathbf{M} is the magnetization, \mathbf{H} is the magnetic field, and \mathbf{D} is the demagnetization tensor.

The MR effect, which is the difference between E with and without magnetic field, normalized with respect to zero magnetic field can be written as

$$\Delta E = \frac{E(\mathbf{H}) - E(H = 0)}{E(H = 0)}. \quad (3.1)$$

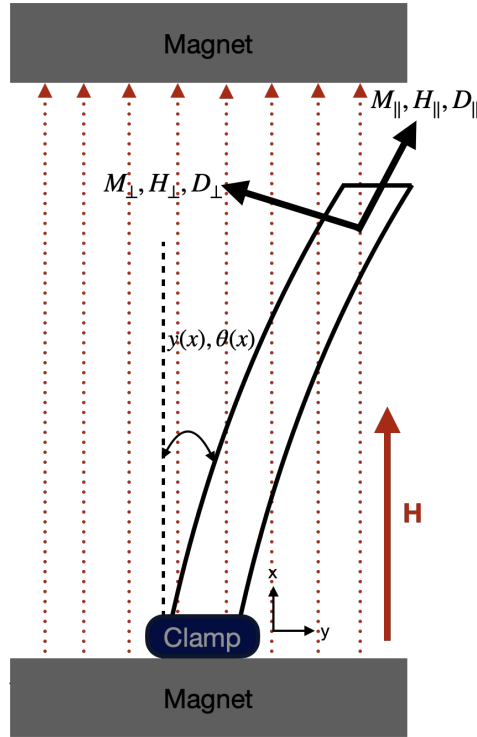


Figure 3.2. Schematic showing the cantilever beam and the parallel and normal components of \mathbf{M} , \mathbf{H} , and \mathbf{D} .

To derive cantilever bending behaviour of MRE, the resultant force exerted by the produced MRE is calculated with the use of superposition principle. The total force consists of elastic and magnetic components

$$F_T(y, H) = F_E(y) + F_H(y, H) \quad (3.2)$$

where F_T is the resultant force at the tip, y is the tip displacement, F_E is the elastic force, and F_H is the force due to magnetic interactions. F_E only depends on y due to material's inherent elasticity while F_H depends on the magnetic field and displacement. When there is no magnetic field ($F_H(y, 0) = 0$), the Equation 3.2 yields $F_T(y, 0) = F_E(y)$, which means there is no magnetic force component at the tip of the MRE sample. This is a valid simplification for soft-magnetic particles like in our case as they have zero remnant magnetization which means material does not have an inherent magnetic stiffness under zero applied field [72]. Their experimental study also indicates that both the elastic and the magnetic components of the resultant force show a nearly linear behaviour with y . Additionally, the experimental data that were collected in this study also showed a linear relation between the resultant force and y , which will be detailed in Section 4.1. The total resultant energy can be found using both magnetic and elastic parts

$$U_T = U_E + U_H \quad (3.3)$$

where U_E and U_H are the potential energy per unit length and magnetic energy density of the beam, respectively.

Using Bernoulli-Euler beam theory, potential energy per unit length of the cantilever beam U_E is given as

$$U_E = \left(\frac{EI}{2} \right) \left(\frac{d^2y}{dx^2} \right)^2 - F_T \left(\frac{dy}{dx} \right) \quad (3.4)$$

where E is the modulus of elasticity of MRE in the absence of a magnetic field and I is the area moment of inertia. Using Bernoulli-Euler theory brings us some limitations about large deformations of hyperelastic materials; however, employing this approach is convenient in our case as it provides us useful metrics to capture the experimental MRE behavior.

The linear magnetic energy density can be written as given in [73]

$$U_H = \mu_0 \left(\frac{1}{2} \mathbf{M} \cdot \mathbf{H} A + \frac{1}{2} \mathbf{M} \mathbf{D} \cdot \mathbf{M} A \right) \quad (3.5)$$

where μ_0 is permeability of the free space, A is the cross sectional area of MRE, \mathbf{M} is the magnetization, and \mathbf{D} is demagnetization tensor. The parallel and normal components of \mathbf{M} , \mathbf{H} , and \mathbf{D} are shown in Figure 3.2. The normal and parallel components of the magnetization of a composite material can be written as

$$M_{\perp} = \frac{\tilde{\chi}}{1 + \tilde{\chi}} H \sin \theta \quad (3.6)$$

$$M_{\parallel} = H \tilde{\chi} \cos \theta \quad (3.7)$$

where $\tilde{\chi}$ is the effective magnetic susceptibility of the MRE.

If we employ a small angle assumption, $dy/dx \sim \theta$, the magnetic energy density can be obtained as

$$U_H = \mu_0 \left\{ \frac{1}{2} \tilde{\chi} H^2 \left[1 - \left(\frac{dy}{dx} \right)^2 \right] + \frac{1}{2} \frac{\tilde{\chi}}{1 + \tilde{\chi}} \left(\frac{dy}{dx} \right)^2 + \frac{1}{2} \left[\frac{\tilde{\chi}}{1 + \tilde{\chi}} \left(\frac{dy}{dx} \right) \right]^2 \right\} A. \quad (3.8)$$

Therefore, total energy per unit length of the beam, U_T , can be obtained as

$$U_T = \mu_0 \left\{ \frac{1}{2} \tilde{\chi} H^2 \left[1 - \left(\frac{dy}{dx} \right)^2 \right] + \frac{1}{2} \frac{\tilde{\chi}}{1 + \tilde{\chi}} \left(\frac{dy}{dx} \right)^2 + \frac{1}{2} \left[\frac{\tilde{\chi}}{1 + \tilde{\chi}} \left(\frac{dy}{dx} \right) \right]^2 \right\} A + \left(\frac{EI}{2} \right) \left(\frac{d^2y}{dx^2} \right)^2 - F_T \left(\frac{dy}{dx} \right). \quad (3.9)$$

The governing differential equation can be captured by minimizing U_T , $dU_T/dx = 0$, which yields

$$\frac{d^3y}{dx^3} - \frac{\mu_0 A c H^2}{EI} \frac{dy}{dx} - \frac{F_T}{EI} = 0 \quad (3.10)$$

where

$$c = \frac{\tilde{\chi}^3}{(1 + \tilde{\chi})^2}. \quad (3.11)$$

The term c is a variable dependent on f of MRE. It is a convenient equation for samples of randomly arranged particles; however, it generally underestimates the effect of c [72]. For soft magnetic particles, $\tilde{\chi}$ can be written as

$$\tilde{\chi} \cong \frac{3f}{1-f} \quad (3.12)$$

which further yields

$$c = \frac{27f^3}{(1-f)(1+2f)^2}. \quad (3.13)$$

The Equation 3.10 was reduced by Lockette *et al.* to be able to find the maximum value of y

$$y = \frac{3F_T}{k} \left[\frac{1}{\psi^2} - \frac{\tanh\psi}{\psi^3} \right] \quad (3.14)$$

where

$$\psi = \sqrt{\frac{3k_H}{k_e}} \quad (3.15)$$

$$k_H = \frac{\mu_0 A c H^2}{L} \quad (3.16)$$

where k_H is the field-induced stiffness of the beam, L is the free length, and k_e is the elastic stiffness of the beam. Again employing the Bernoulli-Euler theory, k_e can be found as

$$k_e = \frac{3EI}{L^3}. \quad (3.17)$$

Additionally, E of composite materials is related to f by the viscosity law [74]. The following formula can be used to evaluate E

$$E = E_0(1 + 2.5f + 14.1f^2) \quad (3.18)$$

where E_0 is the matrix modulus. This equation is valid up to volume fractions of 30% [75]. Equation 3.1 and Equation 3.18 provide us with the information on how applied magnetic field and volume fraction of filler particles affect the rheological behavior of MREs, which is our primary interest.

3.3. Stand-Alone MRE Module

A stand-alone isotropic MRE module has been designed and produced for a proof-of-concept prototype. Since the module that will be applied to the central channel of the STIFF-FLOP is cylindrical, we have also produced the prototype MRE modules as being cylindrical in shape. Dimensions of the prototype MRE can be seen in Figure 3.3.

In total, 12 samples were produced, and initial stiffness change experiments were performed on these prototype modules. The preparation steps and performed experiments are explained in Section 3.3.1 and Section 3.3.2.

3.3.1. Design & Preparation

MRE compounds consist of elastomeric matrix and magnetizable particles, which range from nano to micro sizes. In the previous studies, it was found that softer elastomeric matrices can provide higher MR effect [76]. To be able to observe high stiffness change in the produced MRE, we chose our matrix material as polydimethylsiloxane (PDMS). PDMS is the most extensively used silicon-based organic polymer which can

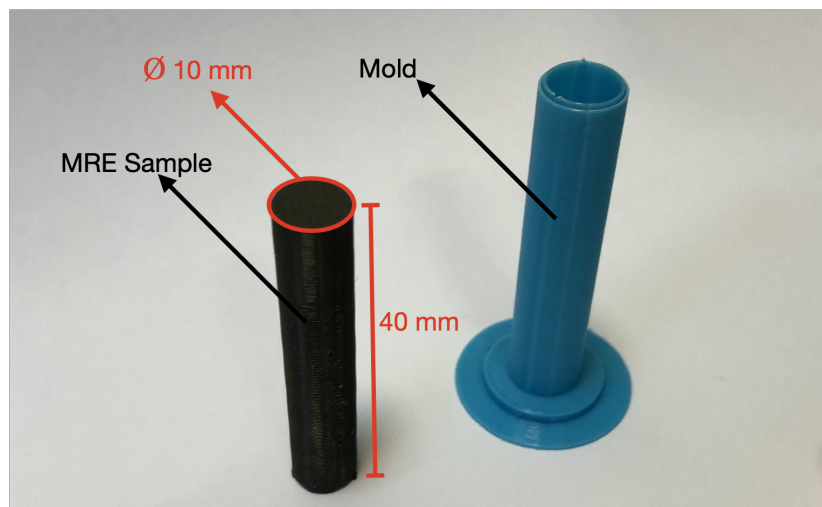


Figure 3.3. A stand-alone isotropic MRE sample with dimensions and production mold.

be categorized under silicones [77]. Non-processed PDMS is an elastic, transparent, and biocompatible material which makes it suitable and applicable to the MIS devices. Sylgard™ 184 silicon elastomer kit was used to produce the MRE samples with 10 to 1 mix ratio of the silicone elastomer base and the curing agent. Production components and molds can be seen in Figure 3.4.

The magnetizable particles were chosen to be carbonyl iron particles (CIP) with an average size of 5 μm . CIP were received from MOLCHEM Inc. with the properties of being spherical in shape and having a purity higher than 99.5%. CIP are classified as soft-magnetic particles, they are one of the most commonly used fillers in MREs. The used magnetic particles have noticeable effect on the rheological behavior of the MREs. The MR effect is improved when the particle size is around 4-5 μm [78]. Additionally, CIP have low remnant magnetization, high permeability, and high saturation magnetization [52], which make them preferable for an enhanced MR effect. Thus, CIP of 5 μm were chosen to use in this study.

To observe the effect of volume fraction of CIP on the mechanical properties of MREs, we produced MRE samples composed of PDMS and CIP of 5 μm . For the reliability of the test samples, we produced 3 samples of each volume fraction, and

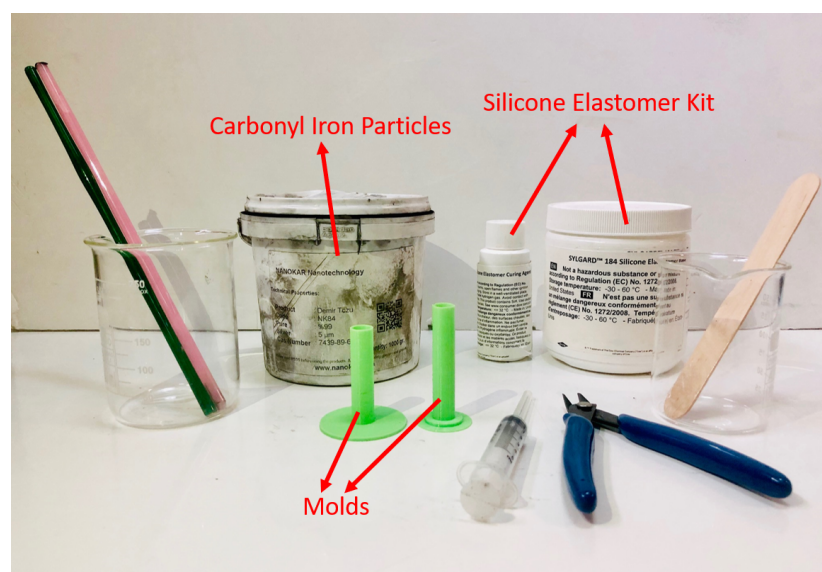


Figure 3.4. MRE production components and molds.

thus 12 in total. The volume fractions of the magnetic particles were 9.09%, 18.18%, 27.27%, and 36.36%.

The initial step while producing the MREs was to mix PDMS compound and magnetic particles thoroughly. The mixture was then directly poured into 3D printed molds made of polyactic acid (PLA). To eliminate the small voids and air bubbles in the samples, they were put under vacuum for approximately 10 minutes. Since the maximum temperature at which PLA molds can withstand is 54°C, the curing process were performed at this temperature for 4 hours. The vacuum oven NUVE EV 18 was used for both vacuuming and curing. Curing was performed without magnetic field in order to have isotropic samples. Thereafter, the samples were removed from the molds and finishing was done using air pressure to distinguish the dust and mold parts from the samples' surfaces. Then, these isotropic MRE samples containing 9.09%, 18.18%, 27.27%, and 36.36% volume fractions were prepared to perform cantilever bending experiments.

3.3.2. Cantilever Bending Experiments

In order to observe the stiffness change of MRE samples, an experimental setup has been constructed using a pulling mechanism and a load cell. The experimental setup can be seen in Figure 3.5. Two identical neodymium permanent magnets of N35 grade with the dimensions of 50 mm × 50 mm × 10 mm with two iron back plates were positioned to face each other. The system holding the magnets is a positioning mechanism which allows to adjust the distance between them, and thus the intensity of the magnetic field traversing the sample in between. The prototype MRE samples with diameter of 10 mm and length of 40 mm were placed on the surface of one permanent magnet with the help of a clamp. The proximal end of the MREs was fixed to the permanent magnet while the distal end was free which allowed us to consider the experiments as cantilever beam experiments.

In these experiments, a micrometer screw gauge with a resolution of 0.01 mm deflected the tip of the MRE samples progressively, and the resulting experimental

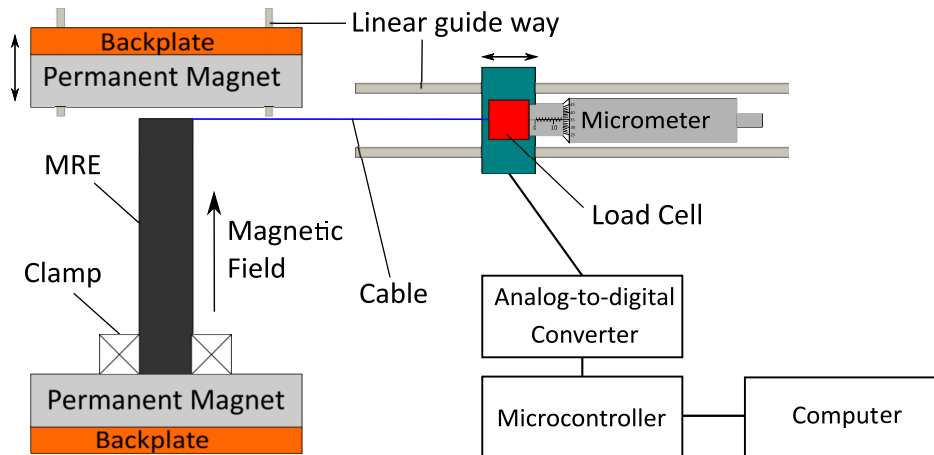


Figure 3.5. Experimental setup for cantilever bending of MRE samples. Micrometer was used to pull a non-extensible cable which was attached to the tip of the MRE sample.

force, F_e , was measured using a 1-kg load cell. F_e measured using Arduino[®] Uno board and its software. The tests were performed for 16 cases; a combination of each sample and four different magnetic fields, which are obtained by changing the distance between magnets. The experiments without an applied external field were conducted by extracting the magnets from the setup, under 0 T. For the experiments of varying external field, distance between magnets were set to 60 mm, 90 mm, and 120 mm. After distances were set, magnetic field measurements were done using a Teslameter (PCE-MFM 2400), and found as 32 mT, 64 mT, and 203 mT for the 120 mm distance, 90 mm distance, and 60 mm distance, respectively. Force measurements for each test were repeated three times to attain reliable test results. Another set of experiments for the MRE applicable to the central channel of the STIFF-FLOP did not performed, it was analyzed with the proposed FEA, which is explained in detail in Section 3.4.

3.4. Finite Element Analysis of the Stand-Alone MRE Module

Considering the modeling difficulties of soft and continuum robots, a possible application of MREs in these robots requires a milli-scale, nonlinear, multiphysics finite element method (FEM) model to analyze stiffness variation at the design stage.

We have developed a multiphysics FEM model in COMSOL[®] Multiphysics software that can be used for different geometries and volume fractions of MRE samples, and varying external magnetic fields. The stand-alone module sizes were directly used in developed model to be able to compare the experimental and the FEA results. After getting matching results which proved that the MREs can help us to modulate stiffness, another model with sizes changed according to the STIFF-FLOP was also developed and the stiffness variation performance of a possible implementation was analyzed.

3.4.1. Model Definition

A 3D model has been constructed using the Magnetostriction node of COMSOL[®]. Magnetostriction explains the change in dimensions of a material according to the change in its magnetization. It is a built-in node which couples both magnetic fields and solid mechanics interfaces under AC/DC and Structural mechanics modules, respectively. It includes the optimal settings for the multiphysics study automatically. If an active multiphysics coupling is not performed, then the material behaves similar to a linear elastic material [79]. Thus, the multiphysics coupling is significant in terms of calculating the effect of magnetic field.

The model is a cylindrical isotropic MRE under the effect of magnetic field created by two permanent magnets, and surrounded by the air domain. The modelled MRE sample has a diameter of 10 mm, and a height of 40 mm. The magnets have a rectangular area of $50 \times 50 \text{ mm}^2$, and a thickness of 10 mm. The model is surrounded by an air domain in order not to violate the electromagnetic field. It is modelled as a sphere with a radius of 100 mm. The geometry of the overall model can be seen in Figure 3.6.

The materials for the air domain and two permanent magnets were directly chosen from the COMSOL[®] material library. Magnets were chosen as neodymium grade N35 (sintered NdFeB). For the modelled MRE, the field dependent E is added as an additional script in MATLAB[®]. MRE is fixed at one end and all other surfaces are free. The prescribed displacement is applied to the MRE from the tip point in the

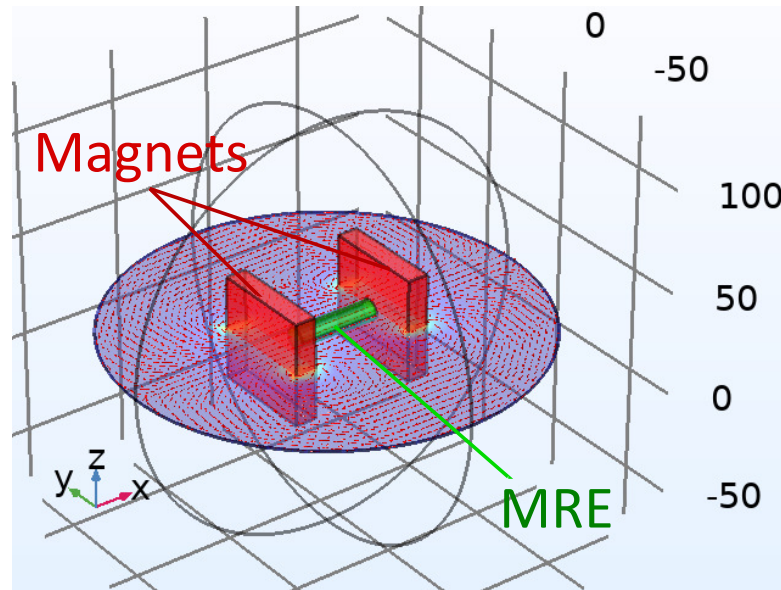


Figure 3.6. 3D model showing magnets (red), an MRE sample (green), surrounding air (grey wireframes), and direction of the magnetic field (red arrows on the xy-plane).

y-direction. The magnets are located in the x-direction as two blocks. The magnetic field is manipulated based on the distance between the two magnets. All domains are included in the magnetic fields interface while only MRE is added to the solid mechanics interface. Both applications of the magnetic field and the tip displacement created a resultant force, which consists of magnetic and elastic forces, in the y-direction. This force is analyzed as it is our primary interest.

From the AC/DC module Magnetic Fields interface, a force calculation was done on MRE to apply the magnetic force part which is occurring due to applied magnetic field. COMSOL[®] performs force calculation on MRE using Maxwell surface stress tensor components. Then, this calculated force was inputted to the MRE as body load. For the postprocessing of the resultant force, we used a node at the tip using Solid Mechanics module, and observed the reaction force in y-direction. Solid Mechanics module only calculates reaction force where there is conditions like fixed constraints or prescribed displacement as in our case. This means that it only includes the elastic bending stiffness. However, as the E of MREs increases due to both k_e and k_H , we added a script that determines E according to these two parameters, then we have analyzed the change in reaction force in y-direction.

We used free tetrahedral mesh for all domains. Mesh element size is set as predefined, “fine” for air domain and “finer” for magnets. For the MRE, we set maximum and minimum element sizes as 5 mm and 0.8 mm, respectively.

3.4.2. Governing Magnetoelastic Equations

A new analytical model was proposed with some improvements made on previous theoretical analysis, detailed in Section 3.2. The governing magnetoelastic equations explained here presents a new analytical model, which were derived based on the fitting of experimental data. This developed analytical model is then integrated into the FEM model, and its validation was done through comparison with the experimental results.

The magnetostriction node describes how an applied magnetic field affects the dimensions of a material. It uses the below constitutive relation which defines the macroscopic properties of the medium using magnetic field and mechanical stress

$$\mathbf{B} = \mu_0[\mathbf{H} + \mathbf{M}(\mathbf{H}, S_{mech}) + \mathbf{M}_r] \quad (3.19)$$

where $\mathbf{M}(\mathbf{H}, S_{mech})$ is material magnetization which depends on the magnetic field and mechanical stress, and \mathbf{M}_r is remnant magnetization which is zero for our material. The mechanical stress in the magnetostrictive material, S_{mech} is automatically modeled in COMSOL[®], using the magnetostrictive strain and the stiffness matrix. For isotropic materials like in our case, this node represents the stiffness matrix in terms of two parameters: Young’s modulus and Poisson’s ratio [79]. Since the stiffness change of the MRE is dominantly characterized by the change in its E , it is important to derive constitutive equations based on this change. As derived in Section 3.2, total force at the tip of the MRE sample can be written as a function of elastic and field induced stiffness.

$$F_T = f(y, k_e, k_H). \quad (3.20)$$

As stated before, E of composite materials is related to f by the viscosity law [74]. However, this equation is inadequate for higher volume fractions [75]. Therefore, the first implementation that were done was to obtain a higher order equation that provided the best fitting for the experimental data, obtained from PDMS-only and four volume fractions of filler particles' cantilever bending experiments. This fit helps us to capture the material behavior at higher volume fractions

$$E = E_0(0.99 + 1.93f + 18.76f^2 - 37.07f^3). \quad (3.21)$$

The Maxwell-Garnett theory aims to approximate a complex electromagnetic medium in terms of permittivity and f . However, it generally underestimates the effect of c in Equation 3.16. As the second implementation to the previous analytical model, We have again fitted experimental data, and established a third order polynomial to calculate the effect of c

$$c = c_1f^3 + c_2f^2 + c_3f + c_4 \quad (3.22)$$

where c_1 , c_2 , c_3 , and c_4 were found using symbolic toolbox of MATLAB[®].

The main contributions that we made to the analytical equations was to derive Equations 3.21 and 3.22 according to our MREs' cantilever bending behavior. These two equations fit better to our experimental data. Thus, we were able to capture MREs rheological behavior more accurately than the study performed by Lockette *et al.* [72].

3.4.3. LiveLink[™] for MATLAB[®]

LiveLink[™] for MATLAB[®] connects COMSOL[®] Multiphysics to the MATLAB[®] environment and enables users to the MATLAB[®] scripting environment. It is possible to create models from a script, arrange the model settings, and also interactive model sharing between COMSOL[®] Desktop and MATLAB[®]. As the solution of the magnetic model and mechanical problem depends on each other, both magnetic fields and solid

mechanics interfaces were automatically coupled, then the results of the magnetic field interface were implemented into the solid mechanics interface. This sequential analysis was performed by adding a script to our model using LiveLink™ for MATLAB® feature.

The first step in creating a finite element model is to create geometry. Geometry settings were adjusted using COMSOL® Multiphysics graphical user interface. Boundary and prescribed displacement conditions were also defined using graphical user interface. MATLAB® script became useful in the solving step. Once the model was created as described in Section 3.4.1, initial solution was imported into the script. In this script, the distance between two magnets, tip displacement, matrix modulus, volume fraction, and geometric parameters were taken as independent parameters. Matrix modulus is defined as 1.6 MPa initially for the MRE from the experimental data, and all other independent parameters can be changed.

First, using the constructed model in COMSOL®, the initial magnet distance is obtained. Also, we have added a magnet distance parameter to one magnet's coordinate in the x-direction. Thus, depending on the distance entered, that parameter in the model is updated and H is calculated. In order for the magnet not to go outside the air domain in the model, we divided the same parameter into two and added it to the surrounding air domain's radius. Geometry parameters are obtained by the same method and it is also possible to enter any dimension that is desired to analyze. To find the stiffness variation of the MRE module, I is calculated in the script according to the model's defined cylindrical geometry. The volume fraction that we want to analyze is then entered.

The script includes a function which takes these parameters as input to calculate E based on governing equations derived in Section 3.4.2 and preset tip displacement. It is possible to change any independent parameter and update the solution accordingly. E is updated automatically in COMSOL® with the help of the script, and corresponding F_T is found for the entered case. The overview of the script can be seen in Figure 3.7. To compare the experimental data and developed model, we first used

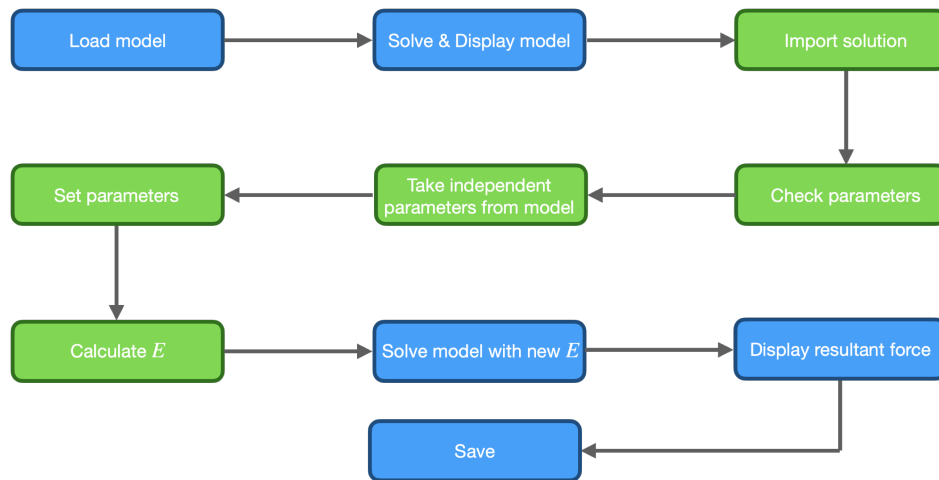


Figure 3.7. Overview of the script used for the resultant force calculations. The blue boxes indicate operations performed in COMSOL[®] while green ones indicate operations performed in MATLAB[®].

the same geometry as the prototype MRE samples. The proposed stiffening module for the STIFF-FLOP manipulator's working channel is also computed with this script.

3.5. Application of the MRE Module to the STIFF-FLOP

The application of the MRE module to the MIS devices can be a promising solution in terms of having higher stiffness variation range and fast response. After proving that MREs can help us modulate stiffness, tunable stiffness of the STIFF-FLOP caused by MREs is also analyzed. The integration consists of two steps: Adapting the MRE to the STIFF-FLOP, and locating the external magnetic field controller according to not to cause a motion-restrictive external effect. The module sizes changed according to fit in the central channel of the STIFF-FLOP. Diameter was reduced to 4.5 mm and the length was extended to 50 mm. The external magnetic field could be manipulated by an electropermanent magnet (EPM), which will be detailed in Section 3.5.2. A possible application of the stand-alone MRE module to the STIFF-FLOP soft manipulator can be seen in Figure 3.8.

To compare the performances of the developed MREs and the currently available solutions, another FEA was also performed with the same dimensions. The central

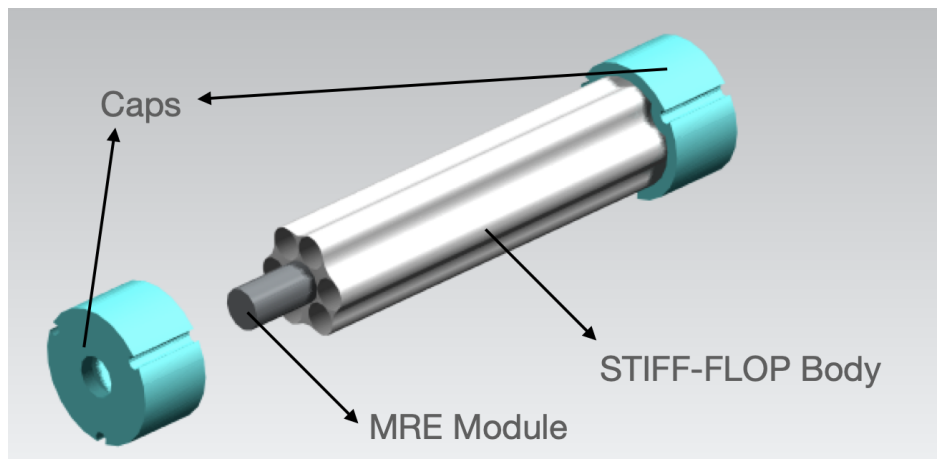


Figure 3.8. A single unit of the STIFF-FLOP showing application of the stand-alone MRE module to the central channel.

channels of the STIFF-FLOP units explained in Section 3.1 are 8 and 9 mm, whereas the module used in this study has a central channel of 4.5 mm. Thus, for a fair comparison, a FEA study for an MRE module of 8 mm in diameter and 50 mm in length was also performed. The stiffness change was analyzed using the developed and implemented script explained in Section 3.4.3. The results are presented in Section 4.2.

3.5.1. FEA for the Implementation

In addition to the FEA of the stand-alone module, another FEA was performed to explore the stiffness values to be obtained with a possible application of the stand-alone MRE at the central channel of the STIFF-FLOP. MRE diameter and length were set to 4.5 mm and 50 mm, respectively. 3D model geometry can be seen in Figure 3.9. The stiffness change under four different magnetic fields, which are 0 T, 32 mT, 64 mT, and 203 mT, and with four different volume fractions, 9.09%, 18.18%, 27.27%, and 36.36%, were analyzed using the developed and implemented script, explained in Section 3.4.3. The cantilever bending behavior of the module applicable to the STIFF-FLOP was observed for these 16 different cases.

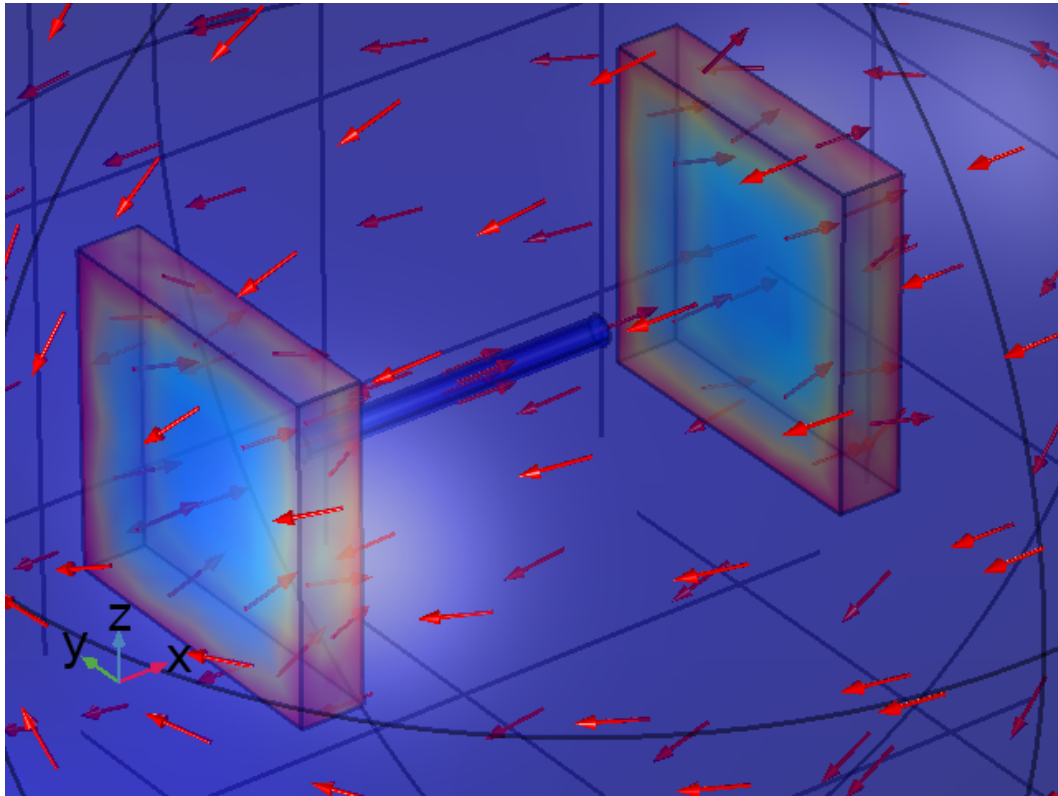


Figure 3.9. FEA of the MRE module applicable to the STIFF-FLOP. Red arrows showing the direction of the magnetic field, MRE module of 4.5 mm in diameter and 50 mm in length is color coded blue at the center of two square magnets.

3.5.2. On-Board Magnetic Field Controller

The critical issue while designing MRE based devices or modules for stiffness variation is the provisioning of magnetic field generator. An on-board magnetic field controller is needed for applications in soft robotics. For the smaller soft robots and manipulators, it is necessary to use external controllers that should not restrict the motion. Using permanent magnets at the design stage was helpful as it is the easiest way to give high magnetic fields to the stand-alone MRE samples; however, they have too many drawbacks as being bulky and unsafe because of their strength. These are some limitations for permanent magnets for the use in soft small manipulators.

Another alternative may be electromagnets but they also require too much power to operate. They also have a heating problem. Thus, the alternative that we chose to

use for providing external magnetic field is EPMs. The EPM is a solid-state device whose external magnetic flux can be turned on and off by a discrete electrical pulse [80]. It was developed by Knaian [80] for magnetically controlling small-scale robotic systems. When the device is in the off-state, NdFeB and AlNiCo magnets are oppositely magnetized. The magnetic flux is only circulating inside of the EPM structure and does not cross the air gap in front of it. When the magnet is on-state, they are magnetized in the same direction and the closed flux circulation goes through the air, through the MRE sample for our case, and creates magnetic field to stiffen the MRE module. The magnetic flux direction when EPM is on-state can be seen in Figure 3.10.

Two EPMs could be sufficient enough to provide needed magnetic field to stiffen the MRE module inside the STIFF-FLOP. In a study performed by Leps *et al.* [81], one EPM with dimensions closer to the designed EPM here is used for MR valve, and they were able to provide 229.4 mT magnetic field density to the valve. Thus, two EPMs could be mounted to the caps at both ends of the STIFF-FLOP soft manipulator so that they match the two ends of the MRE merged in the central channel, and can

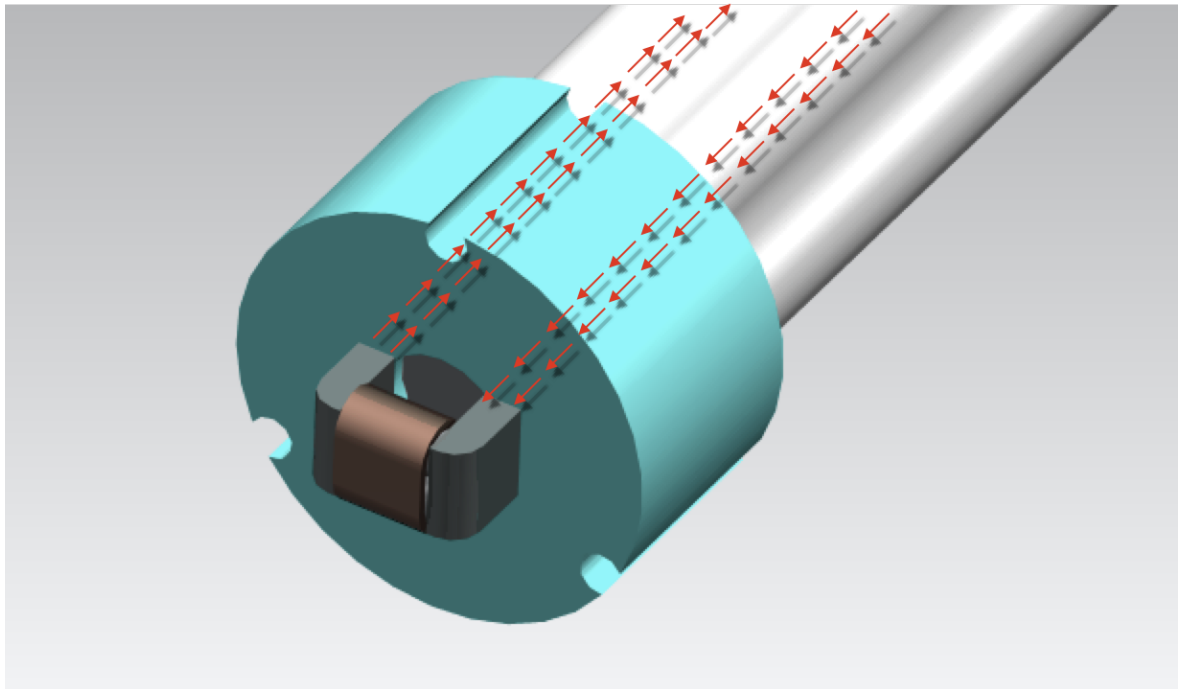


Figure 3.10. A single EPM implemented to the STIFF-FLOP for providing external magnetic field when it is on-state. Red arrows show the circulation of magnetic flux.

provide the needed magnetic field. Geometry of a single EPM and its dimensions can be seen in Figure 3.11. The overall application scenario, which is the implementation of the stand-alone MRE to the STIFF-FLOP and the external magnetic field controllers can be seen in Figure 3.12.

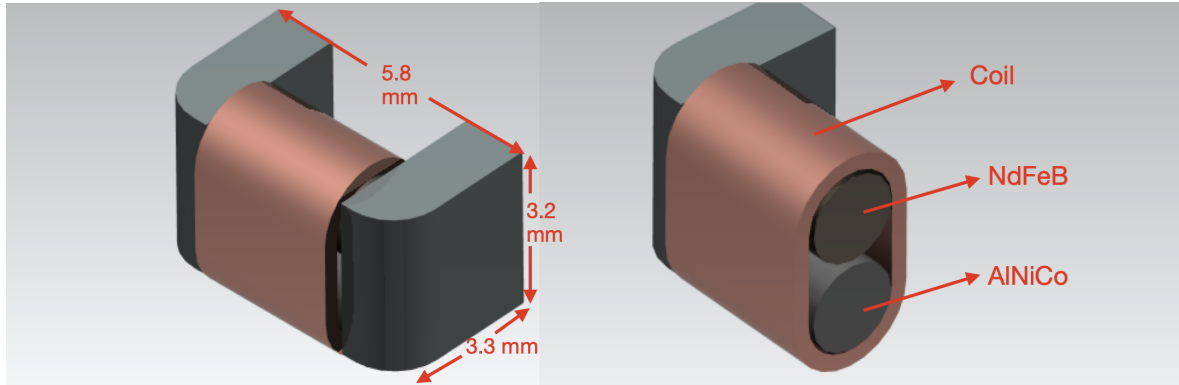


Figure 3.11. Geometry of a single EPM and its dimensions.

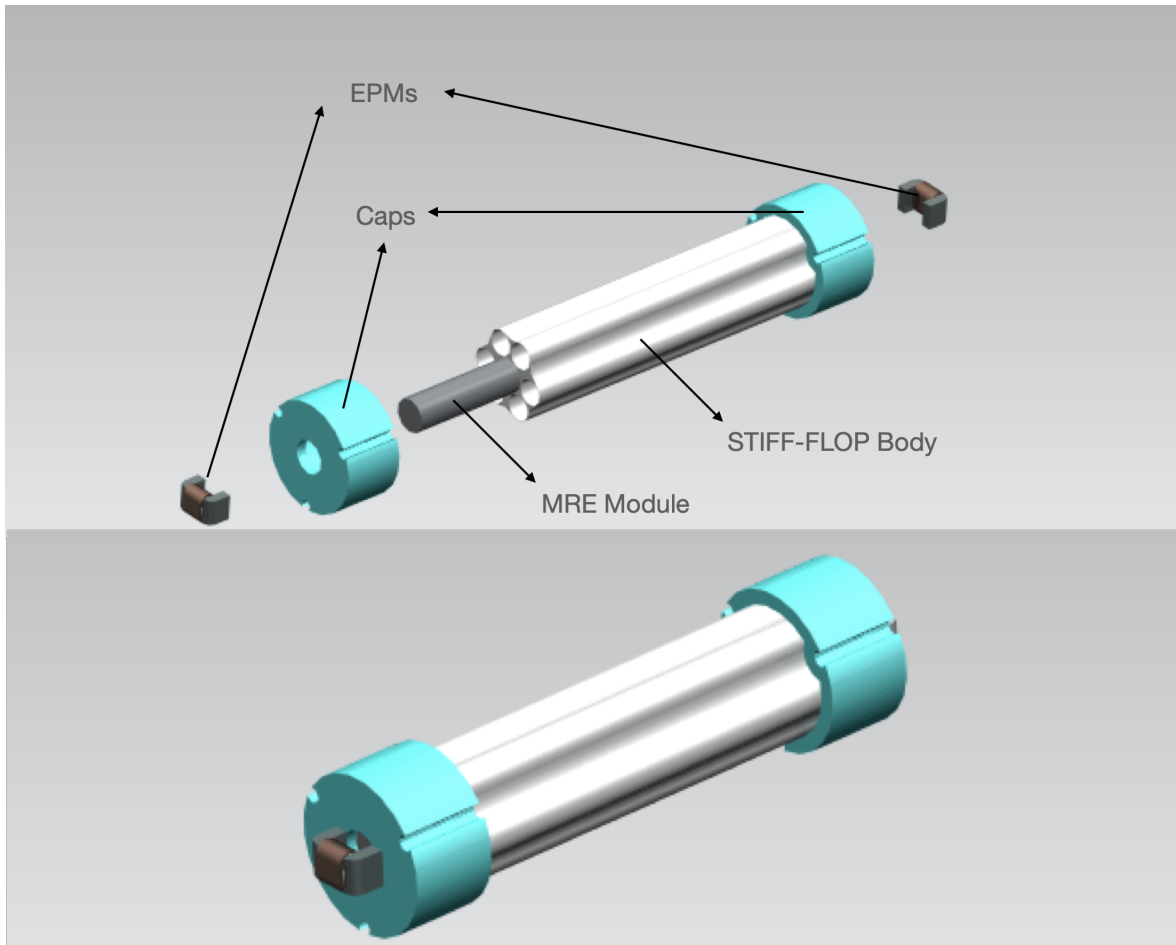


Figure 3.12. The intended application scenario showing the single unit of the STIFF-FLOP merged with developed MRE and external magnetic field controllers (EPMs).

4. RESULTS AND DISCUSSION

The cantilever bending experiment results were presented, and the stiffness change performance of the stand-alone MRE module was analyzed. The results obtained from the experiments were compared with both the analytical model and the developed FEA model. Additionally, the stiffness variation performance of the MRE-based stiffening module applicable to the STIFF-FLOP soft manipulator is introduced again using the developed FEA model.

4.1. Stiffness Change in the Stand-Alone Module

The results of the cantilever bending experiments for four different volume fractions can be seen in Figure 4.1. The error bars presented in Figure 4.1 are not included to the other figures given in Section 4.1.1 and Section 4.1.2, because of clarity issues. However, the experimental data presented in Section 4.1.1 and Section 4.1.2 are the same that are used in this section.

The results indicate that the resultant experimental force (F_e) at the tip shows a nearly linear behavior ($R^2 \geq 0.9943$) with tip displacement for each case. It also increases in direct proportion to increasing volume fraction (f), and magnetic field (T). To illustrate, when tip displacement (y) is 1 cm and no external magnetic field applied, the experimental resultant force measured at the tip of the MRE sample of 9.09% volume fraction is 0.4998 N, while it is 0.937 N for the sample with 36.36% volume fraction. Additionally, for the same tip displacement and volume fractions, the experimental resultant force measured at the tip of the MRE samples under 203 mT magnetic field is 0.6252 N and 1.674 N, respectively. The stiffness values of the stand-alone MRE modules are obtained by comparing the resultant experimental force to a tip displacement of 1 cm. These stiffness values of four different volume fractions under four different magnetic fields are summarized in Table 4.1.

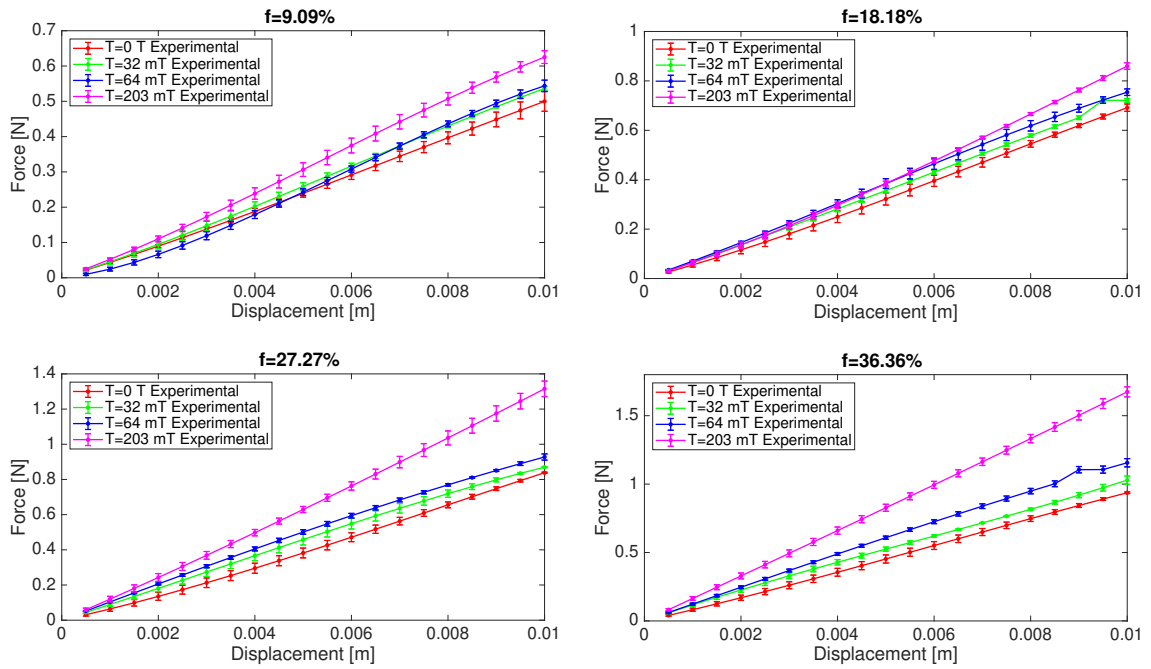


Figure 4.1. Tip force vs. displacement results of the stand-alone MRE modules with volume fractions (f) of 9.09% (top-left), 18.18% (top-right), 27.27% (bottom-left), and 36.36% (bottom-right) under four different magnetic fields (T) (color coded).

Table 4.1. Stiffness [N/cm] values for the stand-alone MRE module.

Volume Fraction (f)	Magnetic Field			
	T0 (0 mT)	T1 (32 mT)	T2 (64 mT)	T3 (203 mT)
9.09%	0.4998	0.5366	0.5438	0.6252
18.18%	0.6915	0.7212	0.7543	0.8601
27.27%	0.8383	0.8699	0.9276	1.315
36.36%	0.9370	1.029	1.156	1.674

In addition to the presented stiffness values, percent change in stiffness is also calculated for each volume fraction. The stiffness values obtained when there is no external magnetic field were used as the base values for each volume fraction. For example, the MRE sample of 9.09% volume fraction, the stiffness value is 0.4998 N/cm, and the percent change in stiffness under the magnetic field was calculated using this value as the base value. The base stiffness values for the MRE samples with volume

fractions of 18.18%, 27.27%, and 36.36% are 0.6915 N/cm, 0.8383 N/cm, and 0.9370 N/cm, respectively. The percent change in stiffness values due to the applied magnetic field is summarized in Table 4.2.

As the column under T_0 presents the base values, the percent change is not applicable (N/A) to them; thus, they have been left as N/A. It can be inferred from Table 4.2 that stiffness change is increasing with the amount of applied magnetic field. Also, for the MRE modules of lower volume fractions such as 9.09% and 18.18%, this increment in stiffness is less than the MRE modules of higher volume fractions. To illustrate, the MRE module of 36.36% volume fraction can change its stiffness up to 78.65% while it is 24.38% for the MRE module of 18.18% volume fraction. The amount of filler particles that the samples contain results in higher field-induced stiffness (k_H). Thus, the rate of change in stiffness in higher volume fractions increases more drastically compared to the rate of change in lower volume fractions. It is stated in the literature that the optimal volume fraction of particles is around 35-40% to have a stronger MR effect [52,60]. We have also observed a higher stiffness change with the MRE module of 36.36% volume fraction. Thus, the stand-alone MRE modules of 36.36% volume fractions can cause stronger MR effect than the lower volume fractions of the MRE modules, and can be used for the possible soft robotics applications.

Table 4.2. Percent change (%) in stiffness [N/cm] values for the stand-alone MRE module obtained from the experiments.

Volume Fraction (f)	Magnetic Field			
	T0 (0 mT)	T1 (32 mT)	T2 (64 mT)	T3 (203 mT)
9.09%	N/A	7.36	8.80	25.09
18.18%	N/A	4.29	9.08	24.38
27.27%	N/A	3.77	10.65	56.86
36.36%	N/A	9.81	23.37	78.65

4.1.1. Analytical vs. Experimental Results

The results of the cantilever bending experiments were compared to the analytical model developed by Lockette *et al.* [72], explained in detail in Section 3.2. The analytical stiffness values were obtained using the slopes of the force vs. displacement curves of the MRE samples, which can be seen in Table 4.3 for 16 different cases. These results were used to calculate the percent error between the analytical and the experimental stiffness values which can be seen in Table 4.4 for 16 different cases. The percent error between the analytical and the experimental results were calculated by

$$\%Error = \frac{F_e - F_a}{F_a} 100. \quad (4.1)$$

The analytical results partially agree with the experimental results for volume fractions of 9.09% and 18.18%. However, the error between the experimental resultant force (F_e) and the analytical resultant force (F_a) is higher for the MRE modules of 27.27% and 36.36% volume fractions. To illustrate, the MRE sample with 9.09% volume fraction the percent error between the experimental and the analytical resultant forces is 1.78, while the rate of error is 36.47 for the sample with 36.36% volume fraction, where both are under zero magnetic field and calculated using Equation 4.1. The results show that the change in stiffness increases with the amount of applied field and volume fraction.

Table 4.3. Stiffness [N/cm] values obtained with the analytical calculations for the stand-alone MRE module.

Volume Fraction (f)	Magnetic Field			
	T0 (0 mT)	T1 (32 mT)	T2 (64 mT)	T3 (203 mT)
9.09%	0.5089	0.5251	0.5260	0.5371
18.18%	0.7486	0.7520	0.7583	0.8326
27.27%	1.0673	1.0722	1.0907	1.3100
36.36%	1.4750	1.4865	1.5264	2.0013

Table 4.4. Percent error (%) between the analytical and experimental results for the stand-alone MRE module.

Volume Fraction (f)	Magnetic Field			
	T0 (0 mT)	T1 (32 mT)	T2 (64 mT)	T3 (203 mT)
9.09%	1.78	2.19	3.38	16.4
18.18%	7.63	4.09	0.53	3.30
27.27%	21.46	18.87	14.95	0.38
36.36%	36.47	30.78	24.27	16.35

In Figure 4.2, comparison of the experimental resultant force and the analytical resultant force at the tip was presented for the MRE sample with 9.09% volume fraction. The results show that for the lower amount of applied magnetic fields, the analytical model is able to capture MRE's field dependent behavior to a greater extent. To illustrate, when there is no applied magnetic field and the tip displacement is 1 cm, the experimental resultant force is 0.4998 N while the analytical resultant force is 0.5089 N. The percent error between these two values is 1.79%, calculated using Equation 4.1. However, for higher external magnetic fields, the results are not as close to each other. For example, when magnetic field is 203 mT and the tip displacement is 1 cm, the experimental resultant force is 0.6252 N, while the analytical resultant force is 0.5371 N. The percent error using Equation 4.1 is 16.4%. Thus, it can be inferred that the analytical method is inadequate for the higher applied magnetic fields. The reason may be the underestimation of the effect of c in Equation 3.16, as explained in Section 3.4.2.

In Figure 4.3, the same comparison between the experimental resulting force and the analytical resulting force at the tip was presented for the MRE sample with 18.18% volume fraction. The highest percent error was obtained when there is no magnetic field applied. The fact that the error is high even when there is no magnetic field means that the analytical model is insufficient even for the elastic part of magnetoelastic equations. In Figure 4.4 and Figure 4.5, the percent error between analytical and experimental stiffness values reach up to 36.47%. The error between the analytical and

experimental resultant forces increases further as the volume fraction increases. This further supports the interpretation that the effect of c in Equation 3.16 is a significant parameter which determines the stiffness change in higher volume fractions.

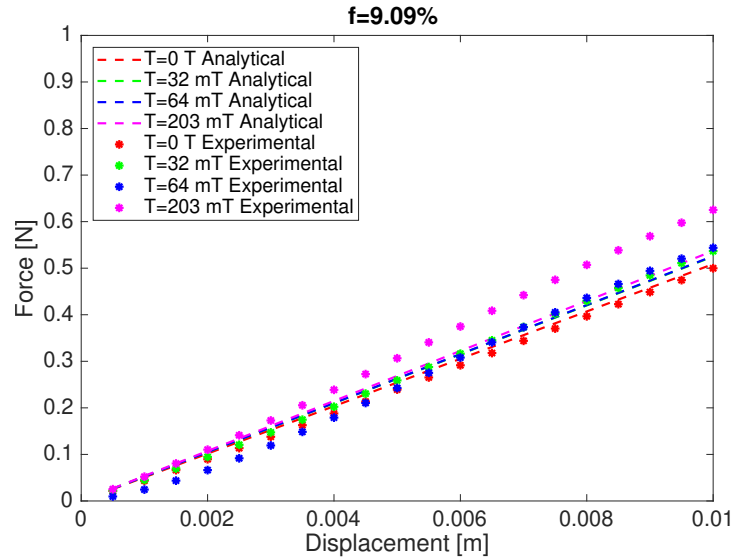


Figure 4.2. Comparison of experimental (dotted data points) and analytical (dashed lines) results: Tip force vs. displacement for the MRE sample of 9.09% volume fraction (f) under four different magnetic fields (T) (color coded).

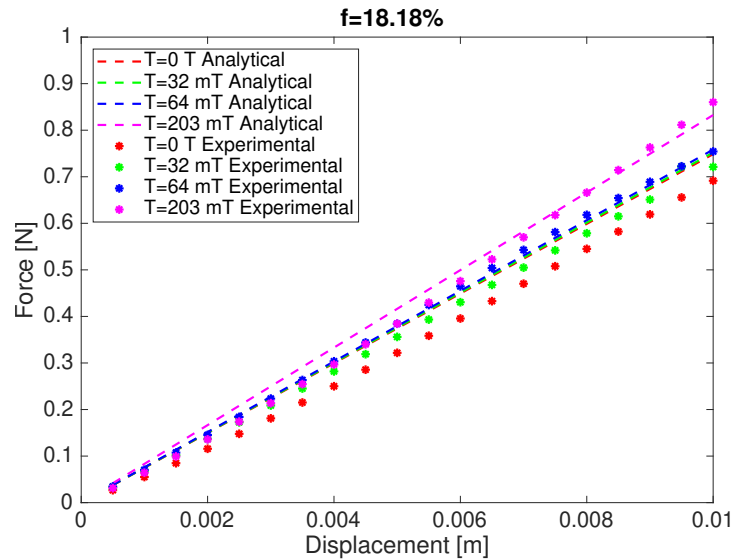


Figure 4.3. Comparison of experimental (dotted data points) and analytical (dashed lines) results: Tip force vs. displacement for the MRE sample of 18.18% volume fraction (f) under four different magnetic fields (T) (color coded).

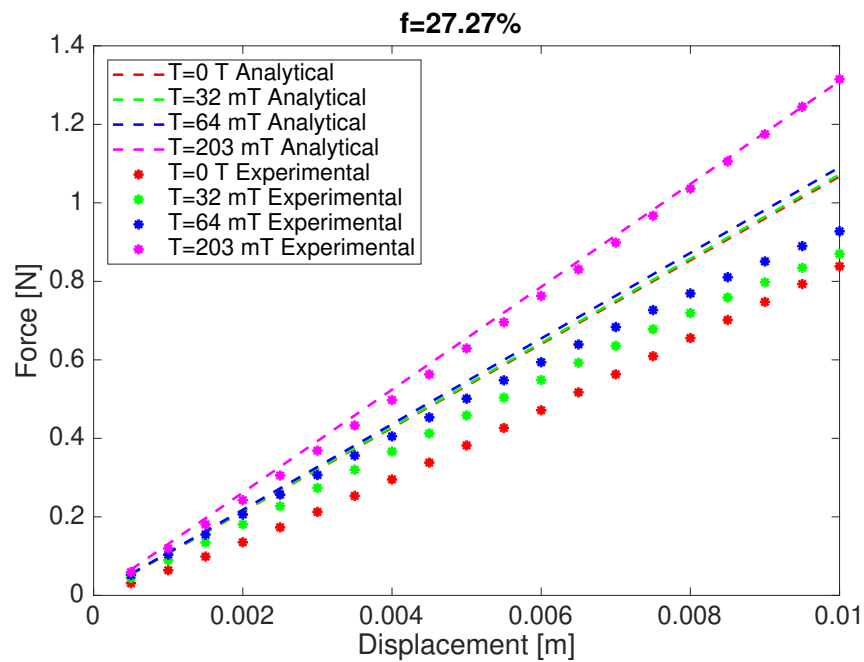


Figure 4.4. Comparison of experimental (dotted data points) and analytical (dashed lines) results: Tip force vs. displacement for the MRE sample of 27.27% volume fraction (f) under four different magnetic fields (T) (color coded).

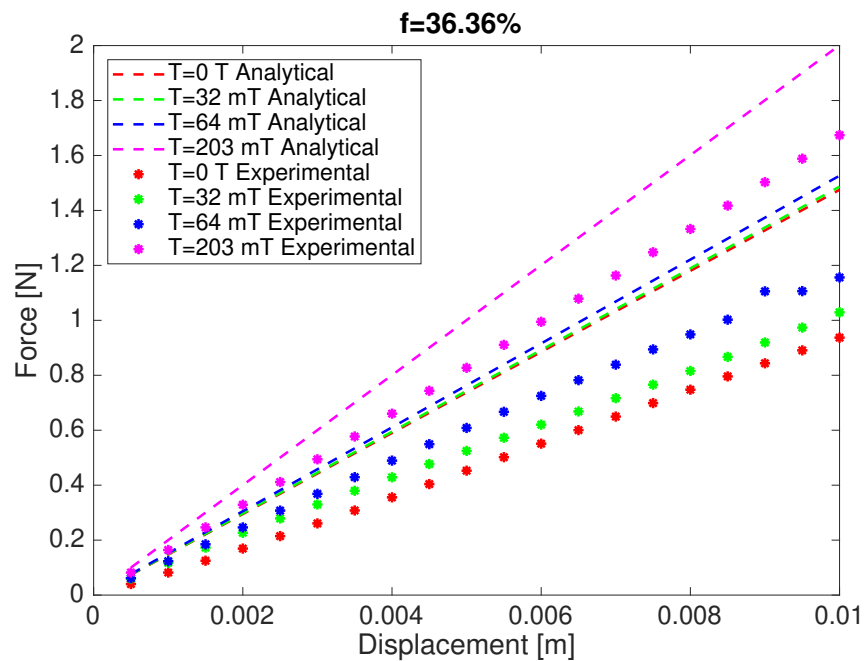


Figure 4.5. Comparison of experimental (dotted data points) and analytical (dashed lines) results: Tip force vs. displacement for the MRE sample of 36.36% volume fraction (f) under four different magnetic fields (T) (color coded).

4.1.2. FEA vs. Experimental Results

After the new analytical model was introduced, and implemented into the FEM model, the comparison between the new analytical model and FEM model were done to observe whether the developed governing equations presented in Section 3.4.2 added to the FEM model correctly. It was observed that the FEA gives exactly the same results that the new analytical model gives, it works with almost zero error. For this reason, no comparison was made between the new analytical model and the experimental results, this comparison was made through the FEA results, as the FEM model includes this new analytical model working in background.

The results of the cantilever bending experiments were compared to the results obtained by the developed FEA model. FEA stiffness values were obtained using the developed script explained in Section 3.4, and the slopes of the force vs. displacement curves of the MRE samples were presented in Table 4.5. These results were used to calculate the percent error between the FEA resultant force (F_T) and the experimental resultant force (F_e) by

$$\%Error = \frac{F_e - F_T}{F_T} 100. \quad (4.2)$$

These error percentages for 16 cases (4 different volume fractions under 4 different magnetic fields) can be seen in Table 4.6.

Table 4.5. Stiffness [N/cm] values obtained with the FEA model for the stand-alone MRE module.

Volume Fraction (f)	Magnetic Field			
	T0 (0 mT)	T1 (32 mT)	T2 (64 mT)	T3 (203 mT)
9.09%	0.5074	0.5099	0.5190	0.6284
18.18%	0.6795	0.6855	0.6998	0.8704
27.27%	0.8449	0.8578	0.8963	1.3534
36.36%	0.9354	0.9550	1.0161	1.7400

Table 4.6. Percent error (%) between the FEA model and experimental results for the stand-alone MRE module.

Volume Fraction (f)	Magnetic Field			
	T0 (0 mT)	T1 (32 mT)	T2 (64 mT)	T3 (203 mT)
9.09%	1.50	5.24	4.78	0.51
18.18%	1.77	5.21	7.78	1.18
27.27%	0.78	1.41	3.49	2.84
36.36%	0.17	7.75	13.77	3.79

The FEA results almost entirely agree with the experimental results for four different volume fractions. To illustrate, for the MRE sample with 9.09% volume fraction the percent error between the FEA and the analytical resultant forces is 1.50; and 0.17 for the sample with 36.36% volume fraction, both under zero magnetic field and calculated using Equation 4.2. The results show that the developed FEA model performs better than the analytical model in capturing the field-dependent material properties of the developed MREs, especially for higher volume fractions.

In Figure 4.6, comparison of the experimental resultant force and the FEA resultant force at the tip was presented for the MRE sample with 9.09% volume fraction. When there is no magnetic field applied and the tip displacement is 1 cm, the experimental resultant force is 0.4998 N, while the FEA resultant force is 0.5074 N. The percent error between these two values is 1.50%, calculated using Equation 4.2. Additionally, when magnetic field is 203 mT and the tip displacement is 1 cm, the experimental resultant force is 0.6252 N, while the FEA resultant force is 0.6284 N. The percent error using Equation 4.2 is 0.51%. Thus, it can be inferred that the developed FEA model is able to capture the produced MREs field-dependent behavior.

In Figure 4.7, the same comparison between the experimental resultant force and the FEA resultant force at the tip was presented for the MRE sample with 18.18% volume fraction. The highest percent error, which is 7.78, was obtained when the external magnetic field is 64 mT. In Figure 4.8 and Figure 4.9, the percent error between

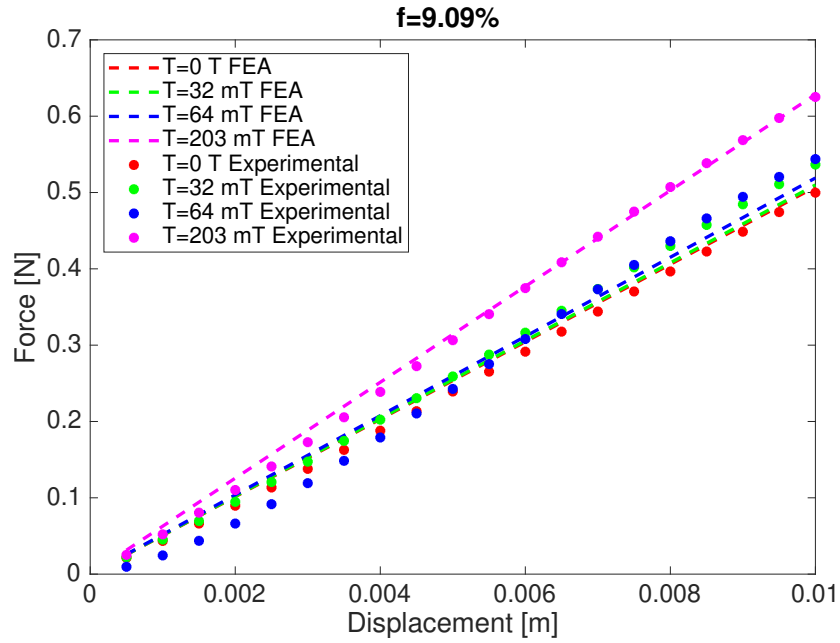


Figure 4.6. Comparison of experimental (dotted data points) and FEA (dashed lines) results: Tip force vs. displacement for the MRE sample of 9.09% volume fraction (f) under four different magnetic fields (T) (color coded).

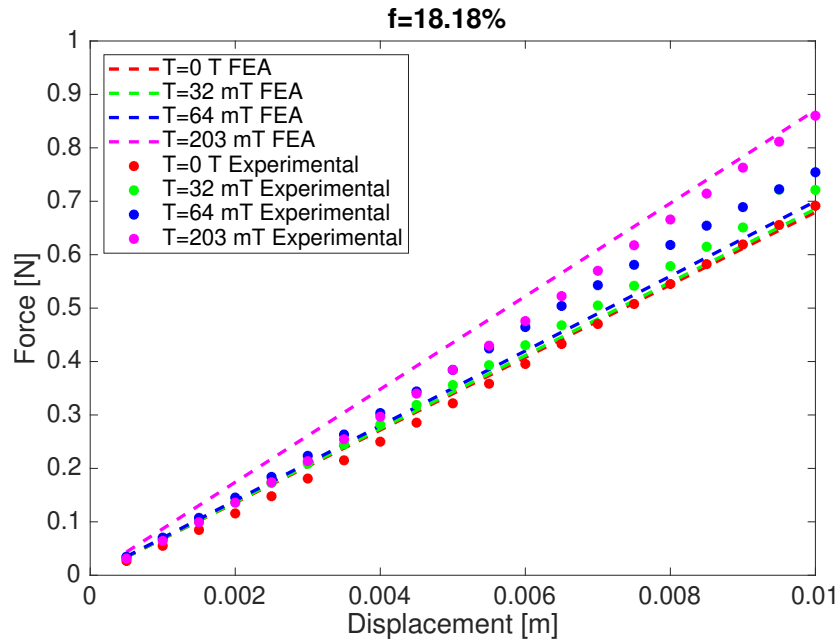


Figure 4.7. Comparison of experimental (dotted data points) and FEA (dashed lines) results: Tip force vs. displacement for the MRE sample of 18.18% volume fraction (f) under four different magnetic fields (T) (color coded).

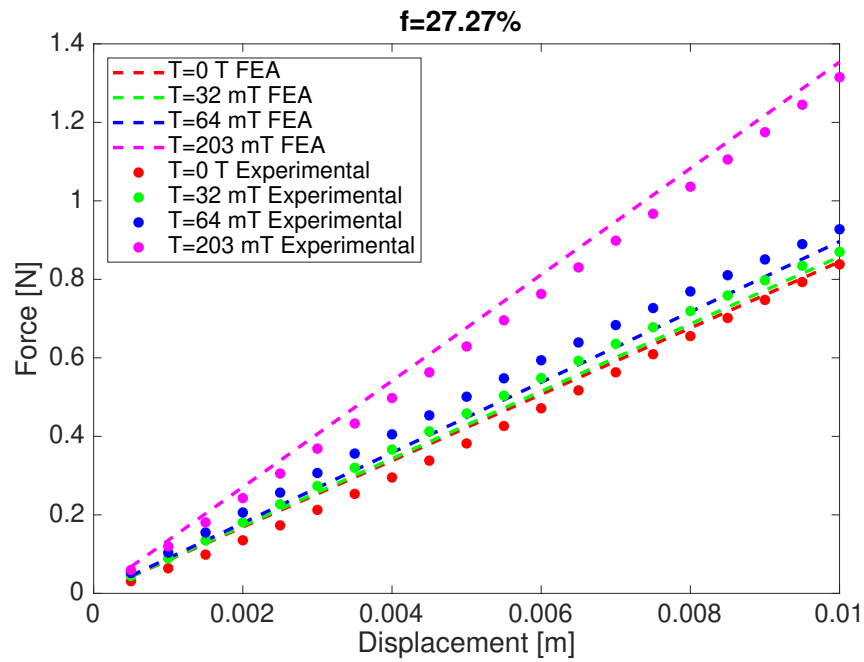


Figure 4.8. Comparison of experimental (dotted data points) and FEA (dashed lines) results: Tip force vs. displacement for the MRE sample of 27.27% volume fraction (f) under four different magnetic fields (T) (color coded).

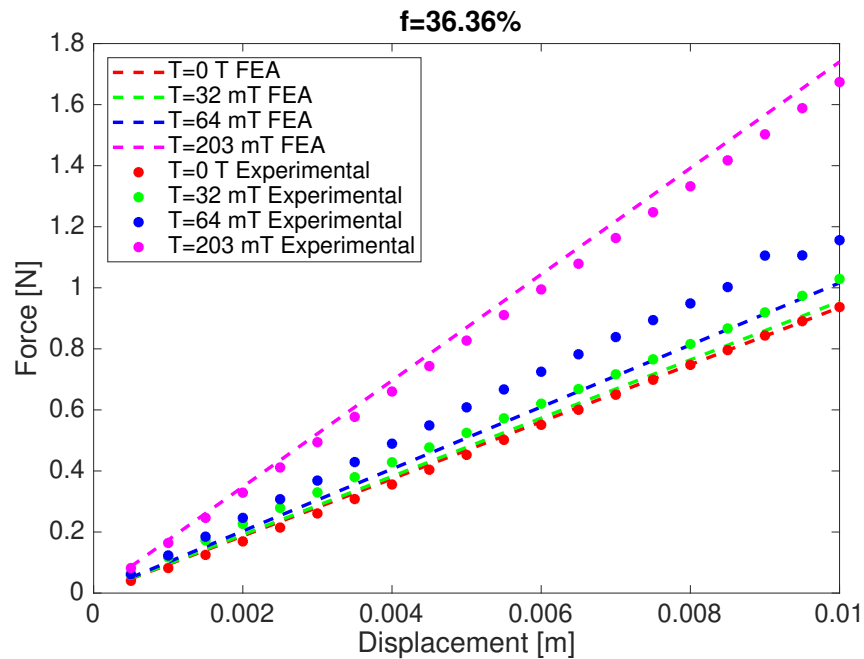


Figure 4.9. Comparison of experimental (dotted data points) and FEA (dashed lines) results: Tip force vs. displacement for the MRE sample of 36.36% volume fraction (f) under four different magnetic fields (T) (color coded).

FEA and experimental stiffness values reaches at most 13.77%, and the nearest value to this error is 7.75%. These error values between the FEA and the experimental resultant forces are far less than the ones obtained by comparing the analytical and the experimental results. This indicates that the developed FEA is more capable of determining the effect of c in Equation 3.16. Therefore, the developed FEA can be used for all volume fractions as the error rates are far less than the analytical model developed by Lockette *et al.* [72], and can be able to capture MREs' material behavior more comprehensively.

Additionally, the results also show that the MRE stiffness increases with higher volume fractions. For instance, the experimental stiffness of the MRE sample with 9.09% volume fraction is calculated as 0.6252 N/cm while the stiffness of the MRE sample with 36.36% volume fraction is calculated as 1.674 N/cm, when magnetic field is 203 mT. The stiffness increases with increasing magnetic field as well. To illustrate, the experimental stiffness of the MRE sample with 27.27% volume fraction is 0.8383 N/cm when there is no applied field, while it is calculated as 1.315 N/cm when applied field is 203 mT.

4.2. Stiffness Change in the Proposed Application

An MRE application to the central channel of the STIFF-FLOP is analyzed with the developed FEA model. The stiffness values of obtained from this intended application can be seen in Table 4.7. The highest stiffness values were obtained with the MRE of 36.36% volume fraction. The percent change in stiffness was also calculated for all of the volume fractions separately, using the zero magnetic field values. The results can be seen in Table 4.8. It was found that the application of an MRE module of 36.36% volume fraction can lead to a 12.83% change in stiffness under 203 mT magnetic field.

The stiffness change values for the stand-alone MREs can reach up to 78.65%; however, for an MRE module applicable to the central channel of the STIFF-FLOP, the maximum change in stiffness is 12.83%. This huge gap between the stand-alone

Table 4.7. Stiffness [N/cm] Values for the Intended Application

Volume Fraction (f)	Magnetic Field			
	T0 (0 mT)	T1 (32 mT)	T2 (64 mT)	T3 (203 mT)
9.09%	0.5069	0.5073	0.5087	0.5266
18.18%	0.6808	0.6815	0.6837	0.7089
27.27%	0.8454	0.8473	0.8531	0.9209
36.36%	0.9352	0.9382	0.9475	1.0552

Table 4.8. Percent change (%) in stiffness [N/cm] values for the MRE applicable to the STIFF-FLOP.

Volume Fraction (f)	Magnetic Field			
	T0 (0 mT)	T1 (32 mT)	T2 (64 mT)	T3 (203 mT)
9.09%	N/A	0.08	0.35	3.89
18.18%	N/A	0.10	0.43	4.13
27.27%	N/A	0.22	0.91	8.93
36.36%	N/A	0.32	1.31	12.83

MRE module and the module that is applicable to the central channel of the STIFF-FLOP may be due to scalability. Since the length is divisor in both the elastic stiffness (k_e) and the field-induced stiffness (k_H) and it is also longer compared to the stand-alone module, we may not have achieved the stiffness values that we expected. The diameter of the central channel of the STIFF-FLOP module presented in [71] is 8 mm as explained in Section 3.1, whereas the module that we have has a central channel of 4.5 mm. For a fair comparison with the same dimensions, we performed an additional FEA study with an MRE module of 8 mm in diameter and 50 mm in length. It was observed that a stiffness change up to 44.26% can be provided with an MRE module of 36.36% volume fraction, under 203 mT applied magnetic field. Thus, the MRE module applicable to the STIFF-FLOP has higher stiffness variation ranges than the already applied methods in the literature. Additionally, there is no need for a pneumatic input and the unstiffening time is faster than the currently available methods. It can also be

proposed that the central channel of the STIFF-FLOP can even be increased to 10 mm, and an MRE with a radius of 10 mm can be implemented to this channel. This can increase the stiffness change up to 78.65% as seen in Table 4.2. This way, the overall system complexity can be decreased, and also the need for continuous power supply can also be removed using EPMS for the manipulation of external magnetic field.

5. CONCLUSION

In this study, a stand-alone MRE module has been developed and analyzed for its applicability to soft robots and manipulators to provide stiffness variation. The developed FEA was used for analyzing a possible application with the STIFF-FLOP soft manipulator, and both FEA results and the analytical results were compared to the experimental ones. The analytical model capturing MREs magnetorheological behavior is further enhanced with an addition to the governing magnetoelastic equations, which explained in detail in Section 3.4.2, and the overall error was reduced. This was succeeded by observing the cantilever bending behavior of MREs in terms of its dependency on the volume fraction of magnetizable particles, and the external magnetic field.

5.1. Contributions and Originality

The originality of this study is provided by the novelty of the FEM model, which is a milli-scale, nonlinear, multiphysics model developed to analyze stiffness variation at the design stage. The main contributions of this FEA model is that the proposed multiphysics model can be used for different geometries and volume fractions of MRE samples, and varying external magnetic fields. In the literature, there is already developed magnetoelastic governing equations that can fit to MREs for cantilever bending case [72]; however, these equations are inadequate for higher volume fraction cases as discussed in Section 4.1.1. The developed FEA is able to capture MREs' unique material behavior more adequately, as it fits better to our experimental data. Additionally, the average error of the stiffness values between analytical and experimental results was 12.68% and it was reduced to 3.87% with the new analytical model. The new analytical model is implemented to the FEA and the comparison between the experimental results and the new analytical model results was done through the FEA results. It was seen that the developed FEA is able to capture MREs' rheological behavior more accurately than the study performed by Lockette *et al.* [72].

Performing experiments for every case is challenging in terms of the difficulties with the equipment; working with strong permanent magnets and creating a magnetic field that is noise-free and unspoilt. This challenge can also be overcome by using our model at the design stage. Additionally, MREs for the stiffness modulation is not explored yet for the STIFF-FLOP; thus, we performed a novel study that can lead to future developments especially for the MIS devices.

This study contributed to the literature as a conference proceeding presenting the FEA model [82].

5.2. Outlook and Future Work

The proposed stand-alone module and the validated FEA are promising for many soft robotics applications that requires fast stiffness change with low power input. The MRE and EPM designs allow for fast response and higher stiffness change values than currently available methods.

Considering the experimental results, we assumed that our material is behaving as a linear elastic material under small strains. This assumption avoids some hyperelastic material features; however, it provided acceptable results as they are really close to our cantilever bending experiment results. Computation time can be decreased as the future work by focusing on simplifying the model or only modeling the quarter of it using the symmetry conditions. Another contribution can be performing more experiments especially for the other stiffness modes like torsion and elongation-compression. They are also delimitative for most of the MIS devices as they should elongate as much as they can.

For possible future applications, an actual implementation can be performed for the STIFF-FLOP to observe the possible imperfections occurring in real world scenarios. Also, additional novel material mechanisms or structural models such as multi-layered MRE design and mechanical metamaterial patterns can be used to have both lower and higher stiffness values, which can increase the overall stiffness range. Also,

anisotropic MREs can provide better MR effect than the isotropic ones as discussed in Section 2.2.1, curing the MREs under a magnetic field can also increase the stiffness variation capability of the stand-alone module. Lastly, providing uniform magnetic field is hard in terms of the need for higher amperes for the electromagnets or the need for stronger magnets and smaller samples. A uniform magnetic field can also increase the overall MR effect and it can be more suitable for the MIS devices.

REFERENCES

1. Laschi, C., B. Mazzolai and M. Cianchetti, “Soft robotics: Technologies and systems pushing the boundaries of robot abilities”, *Science Robotics*, Vol. 1, p. eaah3690, 2016.
2. Majidi, C., “Soft robotics: A perspective—current trends and prospects for the future”, *Soft Robotics*, Vol. 1, pp. 5–11, 2014.
3. Chen, A., R. Yin, L. Cao, C. Yuan, H. Ding and W. Zhang, “Soft robotics: Definition and research issues”, *International Conference on Mechatronics and Machine Vision in Practice*, pp. 366–370, 2017.
4. Manti, M., V. Cacucciolo and M. Cianchetti, “Stiffening in soft robotics: A review of the state of the art”, *IEEE Robotics Automation Magazine*, Vol. 23, No. 3, pp. 93–106, 2016.
5. Liu, T. and Y. Xu, “Magnetorheological elastomers: Materials and applications”, *Smart and Functional Soft Materials*, pp. 147–180, IntechOpen, 2019.
6. Sun, S., J. Yang, W. Li, H. Du, G. Alici, T. Yan and M. Nakano, “Development of an isolator working with magnetorheological elastomers and fluids”, *Mechanical Systems and Signal Processing*, Vol. 83, pp. 371–384, 2017.
7. Cianchetti, M., T. Ranzani, G. Gerboni, I. De Falco, C. Laschi and A. Menciassi, “STIFF-FLOP surgical manipulator: Mechanical design and experimental characterization of the single module”, *IEEE/RSJ International Conference on Intelligent Robots and Systems*, pp. 3576–3581, 2013.
8. Yang, Y., Y. Li and y. Chen, “Principles and methods for stiffness modulation in soft robot design and development”, *Bio-Design and Manufacturing*, Vol. 1, No. 1, pp. 14–25, 2018.

9. Fitzgerald, S., G. Delaney and G. Howard, “A review of jamming actuation in soft robotics”, *Actuators*, Vol. 9, p. 104, 2020.
10. Steltz, E., A. Mozeika, N. Rodenberg, E. Brown and H. Jaeger, “JSEL: Jamming skin enabled locomotion”, *IEEE/RSJ International Conference on Intelligent Robots and Systems*, pp. 5672–5677, 2009.
11. Steltz, E., A. Mozeika, J. Rembisz, N. Corson and H. Jaeger, “Jamming as an enabling technology for soft robotics”, *Electroactive Polymer Actuators and Devices*, Vol. 7642, p. 764225, 2010.
12. Brown, E., N. Rodenberg, J. Amend, A. Mozeika, E. Steltz, M. R. Zakin, H. Lipson and H. M. Jaeger, “Universal robotic gripper based on the jamming of granular material”, *Proceedings of the National Academy of Sciences*, Vol. 107, No. 44, pp. 18809–18814, 2010.
13. Amend, J. R., E. Brown, N. Rodenberg, H. M. Jaeger and H. Lipson, “A positive pressure universal gripper based on the jamming of granular material”, *IEEE Transactions on Robotics*, Vol. 28, No. 2, 2012.
14. Loeve, A., P. Breedveld and J. Dankelman, “Scopes too flexible...and too stiff”, *IEEE Pulse*, Vol. 1, No. 3, pp. 26–41, 2010.
15. Ranzani, T., G. Gerboni, M. Cianchetti and A. Menciassi, “A bioinspired soft manipulator for minimally invasive surgery”, *Bioinspiration & Biomimetics*, Vol. 10, 2015.
16. Cianchetti, M., T. Ranzani, G. Gerboni, T. Nanayakkara, K. Althoefer and P. Dasgupta, “Soft robotics technologies to address shortcomings in today’s minimally invasive surgery: The STIFF-FLOP approach”, *Soft Robotics. (SoRo)*, Vol. 1, pp. 122–131, 06 2014.
17. Santiago, J. L. C., I. S. Godage, P. Gonthina and I. D. Walker, “Soft robots and

- kangaroo tails: Modulating compliance in continuum structures through mechanical layer jamming”, *Soft Robotics*, Vol. 3, No. 2, pp. 54–63, 2016.
18. Kim, Y.-J., S. Cheng, S. Kim and K. Iagnemma, “A novel layer jamming mechanism with tunable stiffness capability for minimally invasive surgery”, *IEEE Transactions on Robotics*, Vol. 29, No. 4, pp. 1031–1042, 2013.
 19. Ibrahimi, M., L. Paternò, L. Ricotti and A. Menciassi, “A layer jamming actuator for tunable stiffness and shape-changing devices”, *Soft Robotics*, Vol. 8, No. 1, pp. 85–96, 2021.
 20. Wang, T., J. Zhang, Y. Li, J. Hong and M. Y. Wang, “Electrostatic layer jamming variable stiffness for soft robotics”, *IEEE/ASME Transactions on Mechatronics*, Vol. 24, No. 2, pp. 424–433, 2019.
 21. Jadhav, S., M. R. A. Majit, B. Shih, J. P. Schulze and M. T. Tolley, “Variable stiffness devices using fiber jamming for application in soft robotics and wearable haptics”, *Soft Robotics*, Vol. 0, No. 0, p. null, 0.
 22. Brancadoro, M., M. Manti, S. Tognarelli and M. Cianchetti, “Preliminary experimental study on variable stiffness structures based on fiber jamming for soft robots”, *IEEE International Conference on Soft Robotics (RoboSoft)*, pp. 258–263, 2018.
 23. Cheng, N., A. Gopinath, L. Wang, K. Iagnemma and A. Hosoi, “Thermally tunable, self-healing composites for soft robotic applications”, *Macromolecular Materials and Engineering*, Vol. 299, 2014.
 24. Shanmuganathan, K., J. R. Capadona, S. J. Rowan and C. Weder, “Stimuli-responsive mechanically adaptive polymer nanocomposites”, *ACS Applied Materials & Interfaces*, Vol. 2, No. 1, pp. 165–174, 2010.
 25. Gandhi, F. and S. G. Kang, “Beams with controllable flexural stiffness”, *Smart*

- Materials and Structures*, Vol. 16, p. 1179, 2007.
26. Shintake, J., B. Schubert, S. Rosset, H. Shea and D. Floreano, “Variable stiffness actuator for soft robotics using dielectric elastomer and low-melting-point alloy”, *IEEE/RSJ International Conference on Intelligent Robots and Systems (IROS)*, pp. 1097–1102, 2015.
 27. Yang, Y., Y. Chen, Y. Li, M. Z. Chen and Y. Wei, “Bioinspired robotic fingers based on pneumatic actuator and 3D printing of smart material”, *Soft Robotics*, Vol. 4, No. 2, pp. 147–162, 2017.
 28. Yuen, M. C., R. A. Bilodeau and R. K. Kramer, “Active variable stiffness fibers for multifunctional robotic fabrics”, *IEEE Robotics and Automation Letters*, Vol. 1, No. 2, pp. 708–715, 2016.
 29. Chenal, T., J. C. Case, J. Paik and R. Kramer, “Variable stiffness fabrics with embedded shape memory materials for wearable applications”, *IEEE/RSJ International Conference on Intelligent Robots and Systems*, pp. 2827–2831, 2014.
 30. Firouzeh, A., M. Salerno and J. Paik, “Stiffness control with shape memory polymer in underactuated robotic origamis”, *IEEE Transactions on Robotics*, Vol. 33, No. 4, pp. 765–777, 2017.
 31. Brodbeck, L. and F. Iida, “An extendible reconfigurable robot based on hot melt adhesives”, *Autonomous Robots*, Vol. 39, pp. 87–100, 06 2015.
 32. Suzumori, K., S. Wakimoto, K. Miyoshi and K. Iwata, “Long bending rubber mechanism combined contracting and extending fluidic actuators”, *IEEE/RSJ International Conference on Intelligent Robots and Systems*, pp. 4454–4459, 2013.
 33. Nagase, J., S. Wakimoto, T. Satoh, N. Saga and K. Suzumori, “Design of a variable-stiffness robotic hand using pneumatic soft rubber actuators”, *Smart Materials and Structures*, Vol. 20, No. 10, p. 105015, 2011.

34. Shiva, A., A. Stilli, Y. Noh, A. Faragasso, I. D. Falco, G. Gerboni, M. Cianchetti, A. Menciassi, K. Althoefer and H. A. Wurdemann, “Tendon-based stiffening for a pneumatically actuated soft manipulator”, *IEEE Robotics and Automation Letters*, Vol. 1, No. 2, pp. 632–637, 2016.
35. Maghooa, F., A. Stilli, Y. Noh, K. Althoefer and H. A. Wurdemann, “Tendon and pressure actuation for a bio-inspired manipulator based on an antagonistic principle”, *IEEE International Conference on Robotics and Automation*, pp. 2556–2561, 2015.
36. Hassan, T., M. Cianchetti, B. Mazzolai, C. Laschi and P. Dario, “Active-braid, a bioinspired continuum manipulator”, *IEEE Robotics and Automation Letters*, Vol. 2, No. 4, pp. 2104–2110, 2017.
37. Cianchetti, M., M. Calisti, L. Margheri, M. Kuba and C. Laschi, “Bioinspired locomotion and grasping in water: The soft eight-arm OCTOPUS robot”, *Bioinspiration & Biomimetics*, Vol. 10, 2015.
38. Laschi, C., M. Cianchetti, B. Mazzolai, L. Margheri, M. Follador and P. Dario, “Soft robot arm inspired by the octopus”, *Advanced Robotics*, Vol. 26, pp. 709–727, 2012.
39. Henke, M., J. Sorber and G. Gerlach, “Multi-layer beam with variable stiffness based on electroactive polymers”, *Electroactive Polymer Actuators and Devices*, Vol. 8340, pp. 412–424, 2012.
40. Robert H. Sturges, J. and S. Laowattana, “A flexible, tendon-controlled device for endoscopy”, *International Journal of Robotics Research*, Vol. 12, No. 2, pp. 121–131, 1993.
41. Kim, Y. J., S. Cheng, S. Kim and K. Iagnemma, “A stiffness-adjustable hyperredundant manipulator using a variable neutral-line mechanism for minimally invasive surgery”, *IEEE Transactions on Robotics*, Vol. 30, pp. 382–395, 2014.

42. Li, W. H., X. Z. Zhang and H. Du, *Magnetorheological elastomers and their applications*, pp. 357–374, Springer Berlin Heidelberg, Berlin, Heidelberg, 2013.
43. Halsey, T. C., “Electrorheological fluids”, *Science*, Vol. 258, No. 5083, pp. 761–766, 1992.
44. Sadeghi, A., L. Beccai and B. Mazzolai, “Innovative soft robots based on electro-rheological fluids”, *2012 IEEE/RSJ International Conference on Intelligent Robots and Systems*, pp. 4237–4242, 2012.
45. Gawade, S. and A. Jadhav, “A review on electro rheological (ER) fluids and its applications”, *International Journal of Engineering Research & Technology*, Vol. 1, pp. 1–7, 2012.
46. Li, Y., J. Li, W. Li and H. Du, “A state-of-the-art review on magnetorheological elastomer devices”, *Smart Materials and Structures*, Vol. 23, p. 123001, 2014.
47. Majidi, C. and R. Wood, “Tunable elastic stiffness with microconfined magnetorheological domains at low magnetic field”, *Applied Physics Letters*, Vol. 97, pp. 164104–164104, 2010.
48. Carlson, J. and M. Jolly, “MR fluid, foam and elastomer devices”, *Mechatronics*, Vol. 10, pp. 555–569, 2000.
49. Brancati, R., G. Massa and S. Pagano, “Investigation on the mechanical properties of MRE compounds”, *Machines*, Vol. 7, p. 36, 2019.
50. Syam, T., A. Muthalif, A. Salem and A. Hejazi, “3D numerical modelling and analysis of a magnetorheological elastomer (MRE)”, *Journal of Vibroengineering*, Vol. 22, pp. 1251–1265, 2020.
51. Li, Y., J. Li, T. Tian and W. Li, “A highly adjustable magnetorheological elastomer base isolator for applications of real-time adaptive control”, *Smart Materials and*

- Structures*, Vol. 22, p. 095020, 2013.
52. Kallio, M., “The elastic and damping properties of magnetorheological elastomers”, *VTT Publications*, pp. 3–146, 2005.
 53. kui Wu, J., X. Gong, Y. Fan and H. Xia, “Anisotropic polyurethane magnetorheological elastomer prepared through in situ polycondensation under a magnetic field”, *Smart Materials and Structures*, Vol. 19, p. 105007, 2010.
 54. Brostow, W., *Performance of plastics*, SPE books from Hanser Publishers, Hanser/Gardner Publications, 2000.
 55. Li, W. H. and X. Z. Zhang, “A study of the magnetorheological effect of bimodal particle based magnetorheological elastomers”, *Smart Materials and Structures*, Vol. 19, No. 3, p. 035002, 2010.
 56. Galipeau, E. and P. Ponte Castañeda, “The effect of particle shape and distribution on the macroscopic behavior of magnetoelastic composites”, *International Journal of Solids and Structures*, Vol. 49, No. 1, pp. 1–17, 2012.
 57. Ivaneyko, Toshchevnikov, Saphiannikova and Heinrich, “Effects of particle distribution on mechanical properties of magneto-sensitive elastomers in a homogeneous magnetic field”, *Condensed Matter Physics*, Vol. 15, No. 3, p. 33601, 2012.
 58. Gong, X., X. Zhang and P. Zhang, “Fabrication and characterization of isotropic magnetorheological elastomers”, *Polymer Testing - POLYM TEST*, Vol. 24, 2005.
 59. Ginder, J. M., M. E. Nichols, L. D. Elie and S. M. Clark, “Controllable-stiffness components based on magnetorheological elastomers”, *Smart Structures and Materials 2000: Smart Structures and Integrated Systems*, Vol. 3985, pp. 418 – 425, 2000.
 60. Kramarenko, E. Y., A. V. Chertovich, G. V. Stepanov, A. S. Semisalova, L. A.

- Makarova, N. S. Perov and A. R. Khokhlov, “Magnetic and viscoelastic response of elastomers with hard magnetic filler”, *Smart Materials and Structures*, Vol. 24, No. 3, p. 035002, 2015.
61. Ginder, J. M., S. M. Clark, W. F. Schlotter and M. E. Nichols, “Magnetostrictive phenomena in magnetorheological elastomers”, *International Journal of Modern Physics B*, Vol. 16, No. 17n18, pp. 2412–2418, 2002.
62. Zhou, G. Y., “Shear properties of a magnetorheological elastomer”, *Smart Materials and Structures*, Vol. 12, No. 1, pp. 139–146, 2003.
63. Chen, L., G. Ae, J. Ae, Y. Ae, D. Ae and W.-H. Li, “Investigation on magnetorheological elastomers based on natural rubber”, *Journal of Materials Science*, Vol. 42, 2007.
64. Roche, J., P. Von Lockette and S. Loffland, “Study of hard-and soft-magnetorheological elastomers (MRE’s) actuation capabilities”, *Proceedings of the 2011 COMSOL Conference in Boston*, COMSOL, Inc. Burlington, MA, 2011.
65. Schubert, G. and P. Harrison, “Large-strain behaviour of magneto-rheological elastomers tested under uniaxial compression and tension, and pure shear deformations”, *Polymer Testing*, Vol. 42, pp. 122–134, 2015.
66. Haldar, K., B. Kiefer and A. Menzel, “Finite element simulation of rate-dependent magneto-active polymer response”, *Smart Materials and Structures*, Vol. 25, p. 104003, 2016.
67. Sun, S., X. Peng and Z. Guo, “Study on macroscopic and microscopic mechanical behavior of magnetorheological elastomers by representative volume element approach”, *Advances in Condensed Matter Physics*, Vol. 2014, pp. 1–8, 2014.
68. Kalina, K. A., P. Metsch and M. Kästner, “Microscale modeling and simulation of magnetorheological elastomers at finite strains: A study on the influence of

- mechanical preloads”, *International Journal of Solids and Structures*, Vol. 102-103, pp. 286–296, 2016.
69. Li, Y. and J. Li, “Finite element design and analysis of adaptive base isolator utilizing laminated multiple magnetorheological elastomer layers”, *Journal of Intelligent Material Systems and Structures*, 2015.
70. De Falco, I., M. Cianchetti and A. Menciassi, “A soft and controllable stiffness manipulator for minimally invasive surgery: preliminary characterization of the modular design”, *IEEE Eng Med Biol Soc*, 2014.
71. Ranzani, T., M. Cianchetti, G. Gerboni, I. De Falco, G. Petroni and A. Menciassi, “A modular soft manipulator with variable stiffness”, *3rd joint workshop on new technologies for computer/robot assisted surgery*, pp. 11–13, Citeseer, 2013.
72. Lockette, P., S. Lofland, J. Biggs, J. Roche, J. Mineroff and M. Babcock, “Investigating new symmetry classes in magnetorheological elastomers: Cantilever bending behavior”, *Smart Materials and Structures*, Vol. 20, p. 105022, 2011.
73. Brown, W., *Magnetostatic principles in ferromagnetism*, Selected topics in solid state physics, North-Holland Publishing Company, 1962.
74. Guth, E., “Theory of filler reinforcement”, *Journal of Applied Physics*, Vol. 16, No. 1, pp. 20–25, 1945.
75. Mullins, L. and N. R. Tobin, “Stress softening in rubber vulcanizates. Part I. Use of a strain amplification factor to describe the elastic behavior of filler-reinforced vulcanized rubber”, *Journal of Applied Polymer Science*, Vol. 9, No. 9, pp. 2993–3009, 1965.
76. Hintze, C., D. Borin, D. Ivaneyko, V. Toshchevnikov, M. Saphiannikova-Grenzer and G. Heinrich, “Soft magnetic elastomers with controllable stiffness: Experiments and modelling”, *KGK Kautschuk Gummi Kunststoffe*, Vol. 67, pp. 53–59, 2014.

77. Wolf, M. P., G. B. Salieb-Beugelaar and P. Hunziker, “PDMS with designer functionalities—properties, modifications strategies, and applications”, *Progress in Polymer Science*, Vol. 83, pp. 97–134, 2018.
78. Wu, C., C. Cheng, A. Abd El-Aty, T. Li, Y. Qin, Q. Yang, S. Hu, Y. Xu and X. Guo, “Influence of particles size and concentration of carbonyl iron powder on magnetorheological properties of silicone rubber-based magnetorheological elastomer”, *Materials Research Express*, Vol. 7, No. 8, p. 086101, 2020.
79. “Magnetostrictive material”, https://doc.comsol.com/5.5/doc/com.comsol.help.sme/sme_ug_theory.06.35.html, Last accessed on 2021-05-20.
80. Knaian, A. N., *Electropermanent magnetic connectors and actuators: devices and their application in programmable matter*, Ph.D. Thesis, Massachusetts Institute of Technology, 2010.
81. Leps, T., P. Glick, D. Ruffatto III, A. Parness, M. Tolley and C. Hartzell, “A low-power, jamming, magnetorheological valve using electropermanent magnets suitable for distributed control in soft robots”, *Smart Materials and Structures*, Vol. 29, No. 10, p. 105025, 2020.
82. Seyidođlu, B., T. Atakuru, K. Uyanık and E. Samur, “Finite element analysis of magnetorheological elastomers for stiffness variation in soft robots”, *4th IEEE International Conference on Soft Robotics (RoboSoft)*, 2021.